University of Stavanger

FACULTY OF SCIENCE AND TECHNOLOGY

MASTER'S THESIS

Study program/ specialization: Offshore Technology/ Marine and Subsea Technology	Spring semester, 2012 Open
Author: Erlend Revheim	…… (signature author)
Faculty supervisor: Eiliv Janssen – UiS External supervisor: Tor-Bjørn Idsøe-Næss – Subsea 7	
Title of Master Thesis: Moonpool operations on Havila Subsea – improvement study	
Credits (ECTS): 30	
Subject headings: Moonpool, Havila Subsea, Prong, Cursor Frame	Pages: 48 + attachments/other: 26 Stavanger, 14/06/2012

This page is intentionally left blank

ABSTRACT

Increasing challenges with regards to remote fields, reservoir conditions and deep water, forces the petroleum industry to adopt new technology. A large part of this technology comes in the form of subsea equipment. Larger and heavier subsea modules are manufactured and installed in order to meet the field and reservoir conditions. Inspection, maintenance and repair (IMR) operations presents a key element in a subsea field life cycle. Lifting through moonpool is preferred when performing such an operation.

A critical factor which has been identified for lifts through moonpool, is when equipment is to be docked onto the cursor frame. During the docking, relative motion between vessel and equipment can lead to large impulse loads. The structural strength of the cursor frame is seen as a limiting factor and a risk element. This is the main reason for Subsea 7 and Statoil to initiate this thesis.

This thesis addresses the module handling system on Havila Subsea. Emphasize has been made on structural challenges of the cursor frame and the possibility of improvement. Both manual capacity calculations and Staad.Pro analysis has been conducted for both existing and alternative cursor frame. The loads have been applied as static loads acting on the tip of the prongs, this is to simulate a worst case scenario where the funnels are just docket at the prongs and the vessel experiences a large pitch or roll motion. The alternative cursor frame has been modeled with new and flexible prongs. The flexible prongs can deflect 5 degrees in any direction.

Analysis shows that the existing cursor frame has a high structural capacity and the prongs are the cursor frame weakest members. The prongs have been proven to have a capacity of 11.8 Te per prong. Effectively this gives a total static cursor frame capacity of 23.6 Te. The flexible prongs have been shown to be beneficial with regards to impulse loads and fatigue. However, for a final recommendation, detailed dynamic analysis and full scale tests are recommended.

Even though structural challenges have been emphasized in this thesis, operational aspects have been regarded and concluding remarks been made.

PREFACE

This thesis is the concluding part of my master degree in Offshore Technology at the Faculty of Science and Technology at the University of Stavanger. The thesis is carried out in cooperation with Subsea 7 S.A. The work has been limited to the period between January – June 2012.

When the work with this thesis started in January 2012, the main objective was to design an improved and flexible prong for use on IMR vessels. During January 2012, Vasshella SMART flexible prong was presented by Espen Pettersen from Vasshella AS. This changed the scope of work from a design analysis thesis into an improvement study with emphasis on the Havila Subsea cursor frame.

The thesis have been solved by a mixture literature study, interview of experienced IMR vessel personnel, hand calculations, software calculations and fieldtrips to Havila Subsea. Calculations have been carried out using MathCad and Staad.Pro. A significant part of this thesis has been put into getting knowledge of the challenges that are valid for moonpool operations on Havila Subsea. Countless hours have been used on mail writing, telephone calls and knocking on office doors, in pursue of updated and relevant documentation. A lot of time has also been used to learn the mathematically software MathCad and the structural analysis software Staad.Pro. In particular Staad.Pro has been time demanding due to problem related to licenses. The work has been carried out at UiS and at the Subsea 7 offices in Dusavik, Stavanger.

I would like to thank my faculty supervisor Eiliv Janssen for all the feedback and guidance during the semester. I would also thank my external supervisor Tor-Bjørn Idsøe-Næss and all other employees at the Naval, Structural and IMR department at Subsea 7 for all the good advice, commitment and support.

Last, I would like to thank my dearest, Elisabeth Tuen for encouragement and advice throughout the thesis and my fellow students Espen Slettebø and Sveinung Rasmussen for all the challenging and interesting discussions.

Erlend Revheim

Stavanger, 14.06.2012

TABLE OF CONTENT

ABBREVIATIONS

The following abbreviations are used in this thesis:

Abbreviation	Definition
AHC	Active Heave Compensation
CF	Cursor Frame
DNV	Det Norske Veritas
EOR	Enhanced Oil Recovery
FCM	Flow Control Module
FEM	Finite Element Method
FPSO	Floating Production Storage and Offloading
GNP	Gross National Product
Hs	Significant wave height
IMR	Inspection, Maintenance and Repair
IOR	Improved Oil Recovery
MHS	Module Handling System
MIT	Multifunctional Intervention Tool
OPEX	Operating Expenses
PwN	Prong with Neoprene
PwS	Prong with Spring
ROV	Remotely Operated Vehicle
RT	Running Tool
SIMO	Simulation of Marine Operations
Staad.Pro	Structural Analysis And Design for Professionals
UiS	University of Stavanger
WOW	Waiting on Weather

LIST OF FIGURES

1 INTRODUCTION

The numbers of subsea developments have been increasing rapidly in the recent years. The low cost of subsea equipment compared to fixed or floating structures is penalized by the difficult availability for inspection, maintenance and repair (IMR). Large maintenance operations are planned to be executed during the summer. However, planned and unplanned maintenance needs to be carried out all year around. This raises the importance for IMR operation to be performed in harsh weather conditions. If maintenance operations are not carried out as planned, severe economical consequences can apply.

Today, more than 50 % of the petroleum produced on the Norwegian continental shelf comes from subsea wells (NPD, 2011). In order to utilize the maximum potential of these wells, safe and cost efficient IMR operations needs to be performed throughout all seasons.

When maintenance one the early subsea fields was performed, whole subsea structures were removed from the seafloor and transported to shore for work over. This led to very large operating expenses (OPEX), and often resulted in fields being developed without subsea wells. New and more sophisticated equipment have opened for faster and more cost efficient maintenance procedures for subsea equipment. Most subsea maintenance these days are preformed at seabed, while the wells are still producing.

The challenges related to offshore lifting operations have been increasing at the same rate as the subsea developments. Larger and heavier equipment are being installed in harsher and deeper water than ever before. These challenges will continue to arise as the oil and gas industry push into Arctic environments and ultra deep waters. Increasing the operating sea state for offshore vessels has a high focus in the industry, this is the main reason for Statoil and Subsea 7 to initiate this master thesis.

In 2010 Acergy initiated a re-rating study for two subsea tools, MIT and FCMRT. This study showed that the recovery phase is the most critical phase during lifting operations thru moonpool (Acergy, 2010). It was shown that relative motion between vessel and RT can result in large loads on funnels and prongs, which in turns can result in damaged equipment and delayed operations.

1.1 Objective

The objective of this thesis is to investigate and highlight the challenges related to Module Handling System of Havila Subsea, specially emphasize on docking of RT funnels onto the CF prongs during recovery phase. Alternative prong design should be checked for feasibility and improvement potential. The result and conclusive remarks made in this thesis should be used as a basis for future discussions regarding launch and recovery of subsea modules through moonpool of Havila Subsea and other similar IMR vessels.

1.2 Methodology

1.2.1 Literature study

A literature study of theory regarding the topic should be performed. The theory presented in the literature study is important to give a wider understanding of the equipment used and challenges present for moonpool operations. Special consideration should be made regarding the functionality of the Havila Subsea MHS, with special attention to loads on the cursor frame.

An introduction into Havila Subsea MHS procedures should be included, with special emphasis on recovery phase and the related challenges.

1.2.2 Hand calculations

A manual calculation of the cursor frame capacities should be included, these capacities should be used as a basis for the detailed structural analysis of the cursor frame. The manual calculations shall be according to Eurocode 3 or NS 3472.

1.2.3 Improvement potential

Improvement of the Havila Subsea MHS should be checked for. Structural problem areas should be described. The improvement check should be based on the Acergy re-runnig study which concluded with; *the most critical issue is the docking of the funnels on the RT onto the prongs on the CF, the small time interval when the RT gets locked to the vessel motions can lead to large tip loads on the prong (Acergy, 2010).*

The flexible prong developed by Vasshella AS should be check for improvement potential.

1.3 Structure of thesis

The main content of this thesis is composed in six chapters, including appendix, of which this is the introduction chapter.

Chapter 2 gives a wide introduction into the literature study performed in this thesis. Relevant theory, challenges and Havila Subsea moonpool handling procedures are presented here.

Chapter 3 describes the structural calculations and analysis performed in this thesis. Results are presented and a brief discussion of the respectively results can be seen.

Chapter 4 discusses all the relevant results and issues which has been discovered during the work of this thesis.

Chapter 5 summarizes all the concluding remarks made by this thesis.

Appendix I-III presents capacity calculations and other relevant calculations performed. Operational issued regarding the flexible prong can be seen in Appendix IV.

1.4 Vessel – Havila Subsea

Havila Subsea was delivered at the 31st of May 2011 from Havyard Leirvik AS to Havila Subcon AS. In June the same year it started on a long term contract between Havila Shipping ASA and Subsea 7. Havila Subsea is a customized IMR vessel and is performing operations on Statoil's subsea field on the Norwegian continental shelf. The vessel is designed to operate in all types of weather conditions and the hull is even designed to withstand light ice conditions.

Havila Subsea is equipped with a 150 Te deck crane, two work class ROVs, one observe ROV and large amount of customized IMR equipment. Havila Subsea has one moonpool measuring 7.2 x7.2 m. This is where the MHS is located and most maintenance and repair operations are operated from.

Figure 1.1 Havila Subsea (Subsea 7, 2011)

Table 1-1 Main characteristics - Havila Subsea

Main characteristics – Havila Subsea	
Length o.a	98.0 m
Length b.p	84.0 m
Breadth	19.8 m
Draft, max	8.0 m
Freeboard	2.0 m

1.5 Havila Subsea – Cursor frame setup

The reason for showing the Havila Subsea – Cursor frame setup, is to give the reader an understanding of important names of cursor frame members used throughout this thesis. Figure 1.2 shows the CF as it lowers an RT through the moonpool during deployment phase.

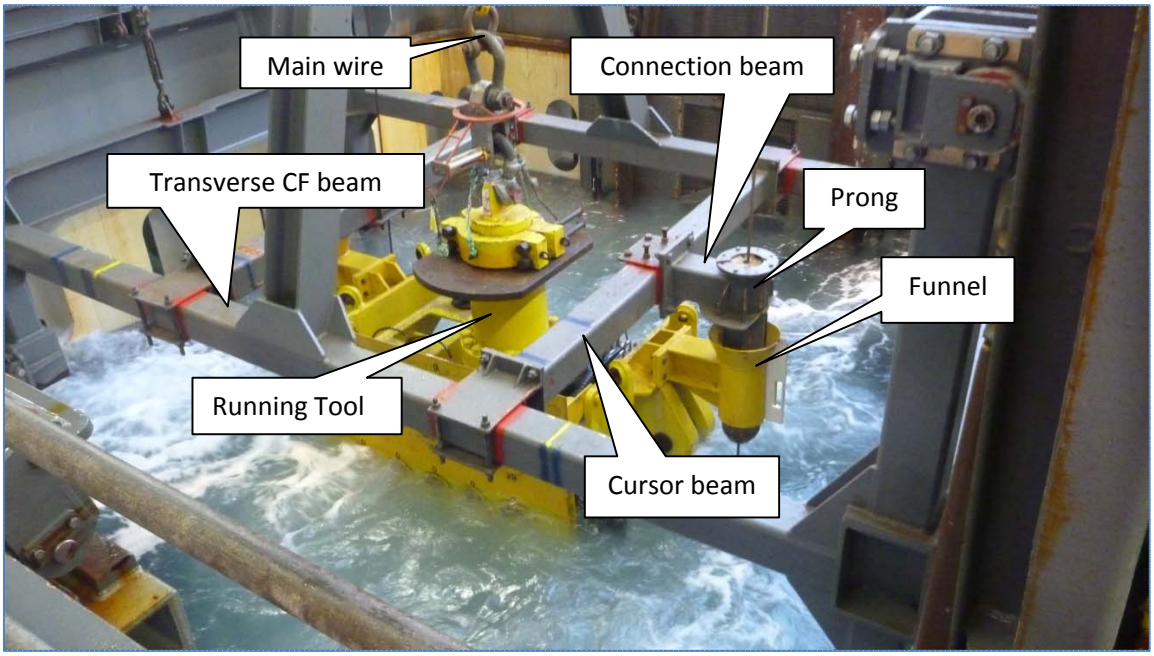

Figure 1.2 Havila Subsea - Cursor frame setup (Heng, 2012)

1.6 Rules and regulations

All activities, operations and design executed and fabricated for petroleum activities in the North Sea, needs to satisfy a strict set of rules and regulations. The Norwegian Petroleum Directorate states the rules and regulations for all the activities being carried out on the Norwegian Continental Shelf.

1.6.1 NS 3472

NS 3472 is the old standard used for dimensioning steel structures. The reason for not using the newer Eurocode 3 is limitation in Staad.Pro code checking is due to the plastic capacities given in Eurocode 3. Since this thesis revolves around the serviceability state of a structure, plastic capacity is of less importance. The code has given the capacities for the steel parts of the system, both elastic and plastic (Norsk Standard, 2001).

1.6.2 DNV Marine Operations

DNV Marine Operations gives the requirements for all ships and vessels performing marine operations. In this thesis DNV have given guidance to how the lifting loads and wave forces affect the subsea modules that are being lifted through the moonpool.

1.7 Computer tool

1.7.1 Staad.Pro

Staad.Pro is a structural analysis and design software which is widely used in the industry. The analysis can give result such as deflections, forces and stresses for the linear elastic area of material behavior. Staad.Pro is capable to perform code check for several different structural codes. In this thesis all the analyses has been performed in Staad.Pro and has been according to NS 3472. The results from these analyses can be seen in chapter 3.3. Staad.Pro was chosen as the analyzing software because of its capability to provide global beam and frame forces. If more detailed local force and stress distributions would have been necessary, ANSYS or another FEM analysis software would have been preferred. The following Staad.Pro facilities have been used:

1. Graphic modeling of the structure.
2. Analysis of deflection forces and stresses.
3. Member utilization checks.

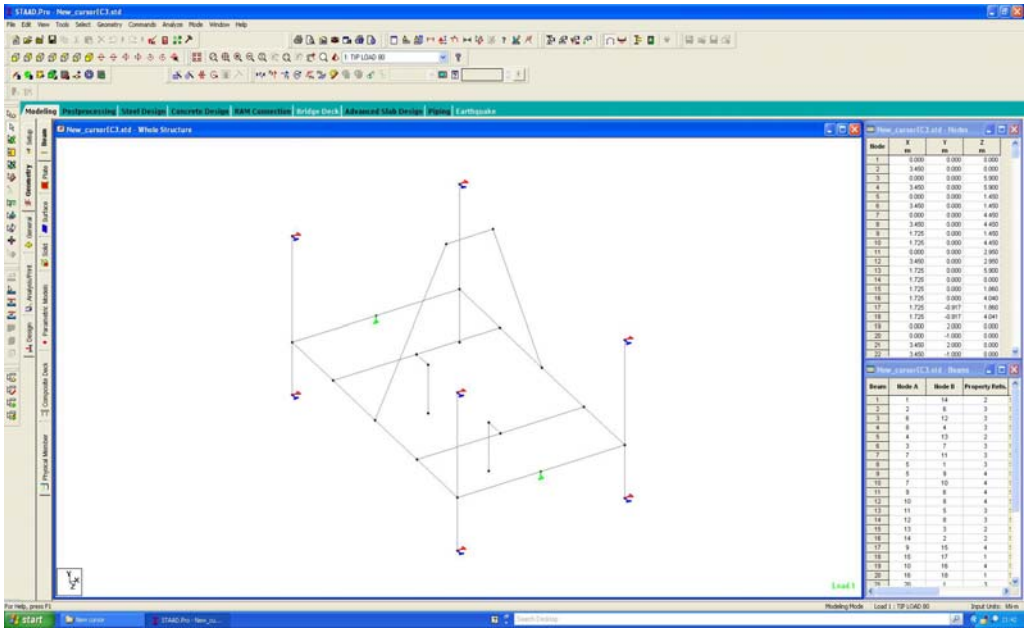

Figure 1.3 Screenshot of Havila Subsea cursor frame model in Staad.Pro

1.7.2 MathCad

MathCad is mathematical software primarily intended for verification and re-use of engineering calculations. It was the first software to introduce live editing of mathematical notations in the calculations. MathCad in widely used by engineering companies across the word.

In this thesis, MathCad have been used substantially. All hand calculations regarding cursor frame capacity, Havila Subsea maximum allowed pitch angle and impulse load calculation have been performed by using MathCad. All of these calculations can be seen in Appendix I, II and III.

2 LITERATURE STUDY – MARINE OPERATIONS AND MOONPOOL THEORY

2.1 Chapter overview

This chapter gives a broad introduction into marine operations, moonpool theory and the importance of this, with regards to Havila Subsea MHS. The reason for this literature study is to place the challenges regarded in this thesis in a big picture. Both challenges and theory in general and specific for Havila Subsea is presented.

2.2 Marine operations

Det Norske Veritas has the following definition of a marine operation:

''…Special planned, non-routine operation of limited duration, at sea. Marine operations are normally related to temporary phases as e.q. load transfer, transportation and installation''
(DNV, 2011b)

Marine operations range from short duration inspection work to long duration pipe-lay operations that can take months to finalize, see Figure 2.1. In the North Sea, all large installations are carried out during the summer months. This is due of the strict weather restrictions prevailing for marine operations. All marine operations are characterized as a weather sensitive operation, hence, large amounts of man hours are spent on planning and optimizing the operational limits. When planning a marine operation, several different challenges need to be accounted for. This is challenges related to vessel availability, sea fastening of equipment and lifts, both inshore and offshore.

For moonpool lifts and operating of the MHS on Havila Subsea, procedures and restrictions for marine operations sets the boundaries.

Figure 2.1 Seven Navica performing a reel pipe-lay (Subsea 7, 2011)

2.2.1 Subsea production equipment

Subsea production systems range from single templates with tie-back to fixed platform, FPSO or shore, to large clusters placed around a manifold, with tie-back to platforms, or directly to onshore facilities. Earlier, mainly small satellite fields where developed using subsea solutions. After years of successfully producing, subsea equipment has proven itself as a safe and cost efficient alternative to the much larger and expensive platform structures. Developments like Ormen Lange and Snøhvit is pushing the limits for next generation subsea oil and gas extraction.

Figure 2.2 Artistic impression of Subsea to Beach Scenario (FMC, 2010)

The equipment used when developing a subsea field is complex and state of the art technology. Every field needs their own tailored made equipment in order to satisfy the reservoir temperature, pressure and depth. All equipment needs to be built in modules so that maintenance and repair can be performed from a surface located vessel. These modules can be, flow control module (FCM), subsea control module (SCM) and many more. The size of these modules is a very important issue, larger modules means large intervention vessel and hence the OPEX increases.

2.2.2 FCMRT & MIT

Some of the most used RT on Havila Subsea is the FCMRT and MIT. This is the same tools that were investigated in the Acergy running tool re-rating study. The RT funnels which interface with the CF prongs can be seen on both Figure 2.3 and Figure 2.4.

2.2.2.1 FCMRT

The Flow Control Module acts as a platform for equipment to regulate and monitor the well flow. At many subsea wells the FCM is also used as a bridge between the X-mas tree and the manifold. The FCMRT is the RT that is used to connect or disconnect the FCM from the X-mas tree. The hydrodynamic properties are not especially good for the FCMRT, this has caused concerns for deployment and recovery through moonpool. There is a variety of configurations of the FCMRT and the FCM system, one configuration is shown in Figure 2.3.

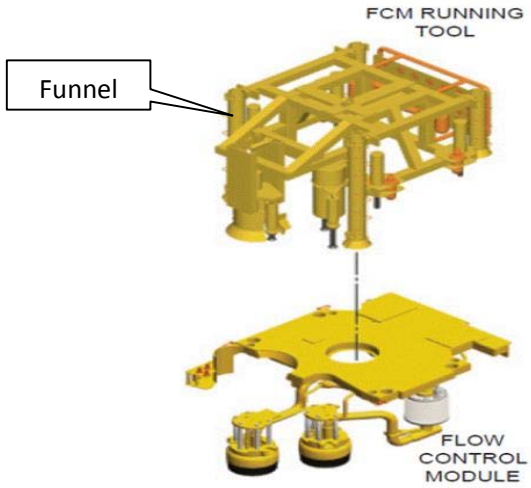

Figure 2.3 Flow Control Module Running Tool (Schjeldrup, 2011)

2.2.2.2 MIT

The Multi Intervention Tool is one of the most used tools on Havila Subsea. The MIT can be used to run subsea control modules and other ``smaller`` subsea equipment. Figure 2.4 show MIT in SCM mode, this means when the MIT is equipped to run a Subsea Control Module.

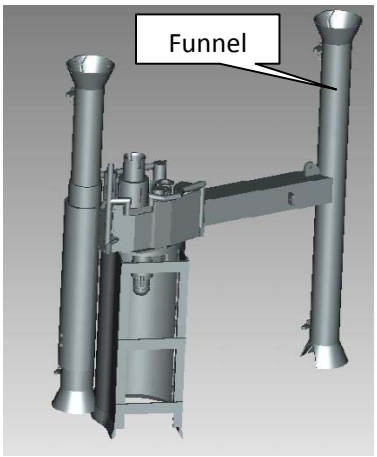

Figure 2.4 Multi Intervention Tool in SCM mode (Acergy, 2010)

2.2.3 Lifting Operations

Offshore lifting operations are performed for many different reasons and in many different situations. They can be performed in connection with new installations, maintenance of platform structures and subsea equipment. Subsea 7 vessels are carrying out lifts for all of the mentioned situations. Common for all lifts are the challenges related to such an operation. A lifting operation can be performed in areas with ultra deep waters, poor visual conditions and be exposed to large waves, currents and winds.

For every lift there is a risk for people and assets. This risk is often increasing with the sea state which the vessel is operating in. In offshore areas like the North Sea, we experience rough and challenging weather conditions in large portions of the year. This can lead to period of WOW and large economical losses for the operating companies can be the consequence. One way of reducing the risk of such a situation, is to have well functioning lifting equipment. For lifts through moonpool this means a well functioning MHS.

For each lift, a large amount of planning is done in advance. This planning consists of risk assessments, lifting analysis with focus on splash zone and snap loads, rigging configuration and deck handling procedures. For large and comprehensive lift the planning phase is much more time consuming than for smaller lifts, DNV-RP-H103 divides offshore lifts into two categories; Light lifts (≤1-2% of vessel displacement) and Heavy lifts (≥1-2% of vessel displacement)(DNV, 2011c).

2.2.3.1 Rigging

Before subsea equipment can be launched from the vessel, a system of lifting devices needs to be attached onto the object being lifted. The equipment used are specific for each lifting operation, shackles, wires, slings, master links and spreader beams are rigging equipment that are commonly used for offshore lifts. Because of the main wires stiff and rigid properties, it's hard to handle. To make the rigging handling easier it is therefore normal to use a soft sling at the lower part of the wire. This also increases the move ability during the lift.

For lifts through moonpool we often see an easier rigging configuration. This is because of the controlled environment that the lift is performed in. The objects being lifted through moonpool are often connected directly to the main wire through a top shackle or a master link. Figure 2.5 shows a normal rigging configuration for a moonpool lift. Here we can see how the lifted object is connected to the main wire through a series of shackles and master links.

Figure 2.5 Moonpool lift - rigging configuration (Heng, 2012)

2.2.3.2 Splash zone

The splash zone or the water entry zone is the phase of a lifting operation when the object being lifted starts to get submerged. In this phase the object can be partly submerged during one wave period. This means that the lowest part of the object can be submerged by the wave crest, at the same time will the upper part of the object be free of water.

Lifting through the splash zone is often one of the most crucial phases of a offshore lifting operation (Gudmestad, 2011). In this phase we often experience the largest hydrodynamic loads, and the crane wire is exposed for snap loads.

2.2.3.3 Snap loads

If the hydrodynamic forces exceed the static weight of a lifted object, the object will suddenly start or stop the lowering velocity or if the main wire goes slack by others reasons, a snap load can be the result. Characteristic snap load may be taken as (DNV, 2011b):

$$F_{snap} = v_{snap}\sqrt{K \cdot (M + A_{33})} \quad [N] \tag{2.1}$$

where

v_{snap} $= characteristic\ snap\ velocity\ [m/s]$
K $= stiffness\ of\ the\ hoisting\ system\ [N/m]$
M $= mass\ of\ object\ in\ air\ [kg]$
A_{33} $= heave\ added\ mass\ of\ object\ [kg]$

Snap loads are of great concern for lifts carried out over the vessel side. For lift through moonpool we have the cursor frame that restricts the object from getting positive buoyancy and therefore also restricting the main wire from going slack.

To minimize the risk of snap load, most offshore cranes are equipped with a heave compensation system. The heave compensation system is installed to avoid heave movements being transferred from the vessel to the main wire.

2.2.4 Weather Window

When planning for construction of platforms and other permanent installations to be placed in a maritime environment it is required to account for extreme weather conditions. We need to design for extreme loads caused by 100 and 1000 years conditions of wind, currents and waves. DNV states that:

- *when planning a marine operation with a reference period exceeding 72 hours, the operation shall be based on extreme value statistical established from historical data or time domain simulations (DNV, 2011c).*

The duration of an operation is determined by the weather conditions that will allow for safe execution. This also needs to include the time needed to safely abort the operation and bring the subsea

equipment into a safe condition[1]. Since an IMR operation normally do not exceed 72 hours we can rely on independent statistical data set by the operator (Statoil) or weather forecasting. In the North Sea most heavy installation lifts are executed during the summer months. IMR operations can, due to the relative small size of equipment, be carried out all year round. When executing lift through moonpool the weather conditions are of even less concern, but even in the sheltered moonpool area there is some limitations.

2.2.4.1 Uncertainty of weather forecasting

Operations which have a planned execution time of less than 72 hours (e.g. IMR), uncertainties in weather forecasting need to be accounted for (DNV, 2011c). The limits for operation (e.g. significant wave height and wind speed) shall be lower than the design values.

In order to calibrate for the uncertainties in weather forecasting, the design criteria should be multiplied with a α-factor. Relevant values for the α-factor for operations in the North Sea and Norwegian Sea is found in DNV-OS-H101.

$$OP_{WF} \leq \alpha \times OP_{Lim} \quad (2.2)$$

where:

$OP_{WF} = operational\ criteria$
$OP_{Lim} = design\ criteria$
$\alpha = calibration\ factor$

Table 2-1 α-factor base case (DNV, 2011a)

Operational Period [h]	Design Wave Height [m]						
	$H_s = 1$	$1 \leq H_s \leq 2$	$H_s = 2$	$2 \leq H_s \leq 4$	$H_s = 4$	$4 \leq H_s \leq 6$	$H_s \geq 6$
$T_{POP} \leq 12$	0.65	Linear Interpolation	0.76	Linear Interpolation	0.79	Linear Interpolation	0.80
$T_{POP} \leq 24$	0.63		0.73		0.76		0.78
$T_{POP} \leq 36$	0.62		0.71		0.73		0.76
$T_{POP} \leq 48$	0.60		0.68		0.71		0.74
$T_{POP} \leq 72$	0.55		0.63		0.68		0.72

[1] In the planning process of a marine operation, guidance can be found in NORSOK N-003 and in the Norwegian Oil Directorate's guides.

2.3 Moonpool

Moonpools are used on many different vessels and rigs. The purpose of the moonpool spans from launch and recovery of subsea equipment, diving bells, ROVs and even cable and riser installation. The moonpool provide the possibility to perform a lifting operation in a sheltered environment, protected from the wind and waves. The moonpool normally consist of straight vertical walls that go from the vessel deck and down to the keel, uniform cross section area. The moonpool is in most cases located close to the vessel roll and pitch axis, this is to minimize the effects from vessel angular motions. On Figure 2.6 we see the basic idea behind lifting through moonpool. However, even though the idea is simple enough, theory related to moonpool operations can get very complex.

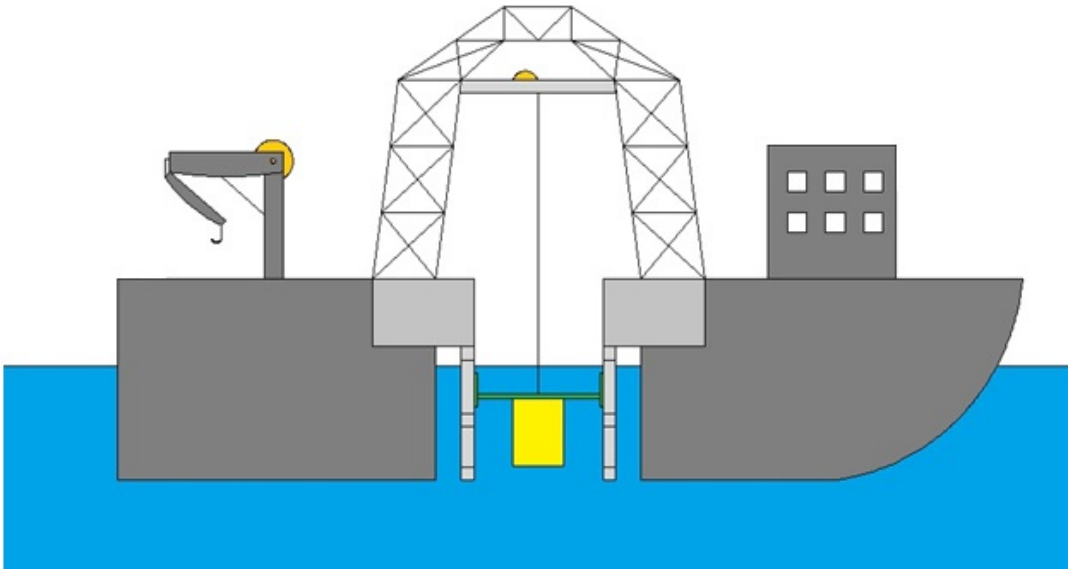

Figure 2.6 Moonpool illustration

2.3.1 Moonpool lifting vs. over side

For a proper designed vessel, the motions in moonpool should be smaller than those experienced over the vessel side. Motions for a vessel are of a six degree of freedom configuration. These motions are divided into translator and angular motions. The translatory motions are referred to as surge, sway and heave, where heave is the vertical motion. The angular motions are referred to as roll, pitch and yaw, with yaw being rotation about a vertical axis. For a ship we have that surge is the longitudinal motion and roll is the angular motion about the longitudinal axis (Faltinsen, 1990).

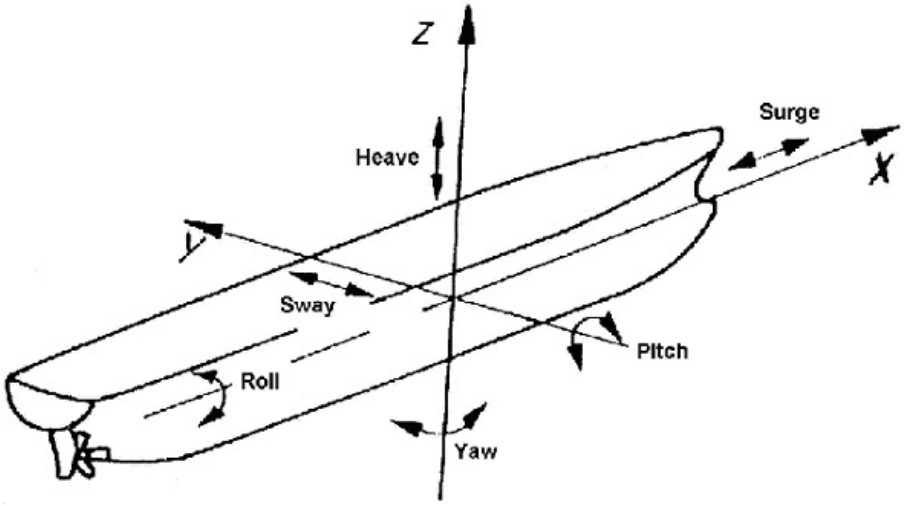

Figure 2.7 Vessel motions (Benedict, 2004)

As described in this thesis, the preferred location for moonpool is near the centre of pitch and roll, this can be proven mathematically(Stald, 2011).

In order to prove this statement we need to look at the equation which describes the motion of any point on the body (Faltinsen, 1990):

$$s = (\boldsymbol{\eta}_1 + z\,\boldsymbol{\eta}_5 - y\,\boldsymbol{\eta}_6)\boldsymbol{i} + (\boldsymbol{\eta}_2 - z\,\boldsymbol{\eta}_4 + x\,\boldsymbol{\eta}_6)\boldsymbol{j} + (\boldsymbol{\eta}_3 + y\,\boldsymbol{\eta}_4 - x\,\boldsymbol{\eta}_5)\boldsymbol{k} \qquad (2.3)$$

here we have that $\boldsymbol{\eta}_i$ denotes displacement in the different directions, 1, 2 and 3 denotes surge, sway and heave, respectively, 4, 5 and 6 denotes roll pitch and yaw, respectively. Since we know that the moonpool is located at the centre of roll and pitch we can say that; $\boldsymbol{\eta}_4 = \boldsymbol{\eta}_5 = \boldsymbol{\eta}_6 = 0$. This gives us a more simplified equation for motion of any point on the body:

$$s = (\boldsymbol{\eta}_1)\boldsymbol{i} + (\boldsymbol{\eta}_2)\boldsymbol{j} + (\boldsymbol{\eta}_3)\boldsymbol{k} \qquad (2.4)$$

Due to the crane tip location away from the centre of roll and pitch, this simplification cannot be performed. As a consequence of this we may expect larger motions and crane tip velocities when lifting over the vessel side.

Another important difference between lifting in moonpool and over the side is the CF. Because of this we have full control over the object as it is being lifted into the sea. This is a big advantage in comparison to the problem related to snap loads when lifting over the side. Table 2-2 shows some advantages and disadvantages for lifting through moonpool.

Table 2-2 Moonpool advantages and disadvantages

Advantages	Disadvantages
Protection of equipment from environmental forces; waves, winds and ice flows.	Water plugs within moonpool can result in flooding of vessel deck and large loads on equipment in moonpool.
No need for lifting of equipment on deck due to skidding system.	Equipment can slam into cursor-frame or get stuck when entering the moonpool.
Moonpool close to vessel roll and pitch axis minimize effect from vessel angular motions during lifting operations.	Size limitations of equipment.

2.3.2 Havila Subsea Module Handling System (MHS)

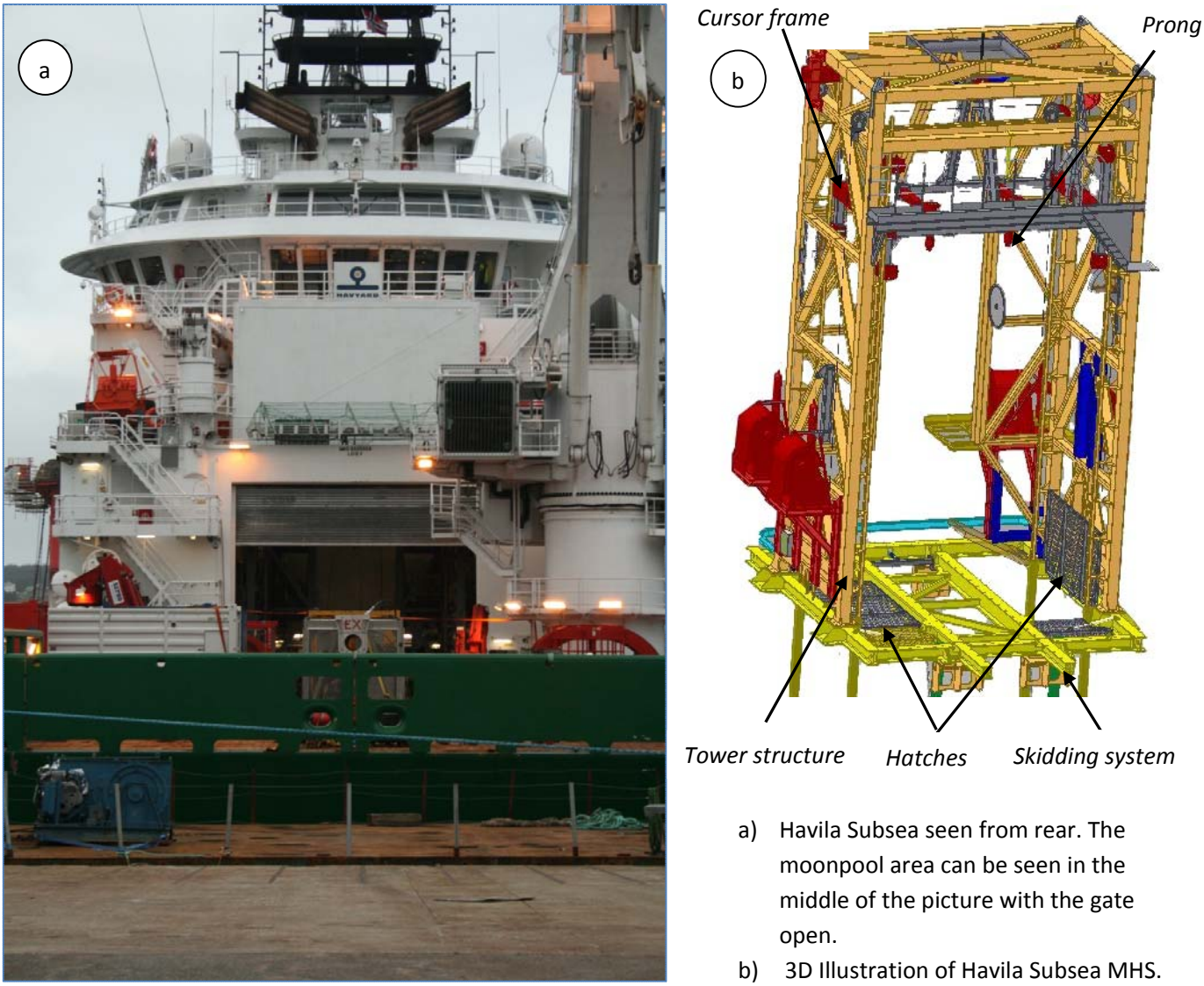

a) Havila Subsea seen from rear. The moonpool area can be seen in the middle of the picture with the gate open.
b) 3D Illustration of Havila Subsea MHS.

Figure 2.8 Havila Subsea from rear and MHS 3D illustration

This subchapter will give an introduction into the main components of Havila Subsea Moonpool Handling System. Chapter 2.4 will go in to the details of how the MHS is operated and challenges related to operations. Figure 2.9 shows an illustration of components in the MHS.

For lifting operations, Havila Subsea deck crane is used as a MHS crane. The deck crane is placed with the crane tip directly above the moonpool area. When the subsea equipment is ready to get lifted, the main wire is pulled through an opening of the moonpool area housing and connected to the subsea equipment.

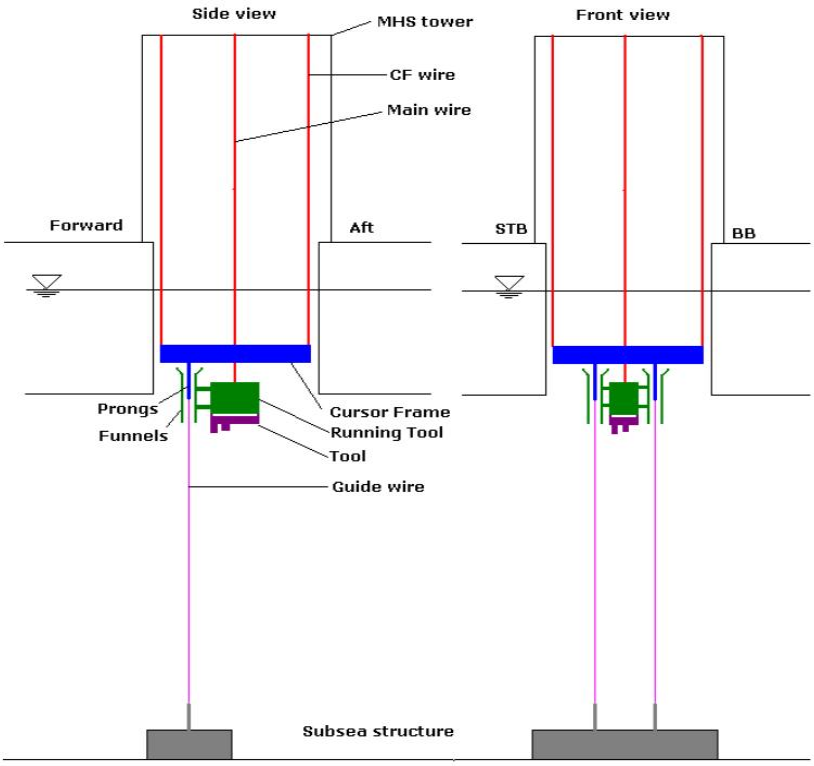

Figure 2.9 MHS - Main components in moonpool system(Acergy, 2010)

2.3.2.1 Tower

The tower structure gives the structural support for all the equipment needed to perform a lift through moonpool. The structure consist of different type of beams, being I-section, H-section and RHS section in different sizes. The steel grade throughout the tower is S355.

The dimensions of the tower is 4.9 x 7.9 x 12.9 m (L x W x H), the height is from the vessel deck up to the tower roof. The tower is supported by four piles going 8.4 m into the vessel structure.

2.3.2.2 Hatches

The hatch system located over the moonpool is consisting of 17 hatches. They are locked in closed position when the moonpool is not in use and locked in open position when the moonpool is being used. The hatches need to take large slamming forces from the water as the vessel is moving. The hatch system on Havila Subsea has shown to be a concern by personnel operating it, this is due to the time consuming, manual opening procedures of all 16 side hatches (the centre hatch is opened by hydraulic). Some concluding remarks are made regarding the hatches in chapter 5.

2.3.2.3 Guiding System

The guiding system consists of all equipment that provides guidance for equipment being lifted through the moonpool. The main components of the guiding system are:

- guide wires
- cursor frame
- prongs

2.3.2.3.1 Guide wire

The guide wires are as the name states; wires that guide the lifted object between the vessel and the seabed. They make sure that the object are landed or docked at the correct location. The guide wires do not have any lifting capacity but they are still exposed to large tension loads. These tension loads occur when the objects get influenced by hydrodynamics forces. The guide wires are also pre tensioned in the docking phase of a lifting operation. This is to ensure a straight and vertical connection between the subsea equipment or vessel and the lifted object. In general one may argue that the tension should be minimized for the deployment operation and maximized for the recovery operation (Acergy, 2010).

The MHS on Havila Subsea have 3 guide wires installed. These can be pre tensioned to 4Te and have an operating length of 1000m. They are controlled manually and follow the main wire lifting speed.

2.3.2.3.2 Cursor frame

The CF consists of several frame beams and two prongs. The main purpose of the CF is to provide a controlled and safe launch and recovery of the lifted object. The cursor frame beams and prongs are moved and placed on different locations for each lift, this is to get aligned with the respective funnels on the subsea equipment. Figure 2.10 shows how the CF holds the object in horizontal direction as it gets lifted through the moonpool splash zone. We can also see the red, blue and yellow markings which show where the beams and prongs have been placed during earlier lifts.

Figure 2.10 Cursor frame support subsea equipment lifted through moonpool (Heng, 2012)

2.3.2.3.3 Prongs

Prongs are the CF guide pins. Havila Subsea is using a prong configuration which involves a steel cape with an oak core. The oak core is to insure lower friction forces between the steel cape and the guide wire. Figure 2.11 shows one of the prongs on Havila Subsea, we see the guide wire going through the prong. The prongs have a pipe cross section made from S355 steel, the dimensions are:

- Prongs length: 900mm
- Outer diameter: 219mm
- Wall thickness: 10mm

The prongs have been identified by several independent sources to be a possible weak part of the CF system (Acergy, 2010) and (Stald, 2011).

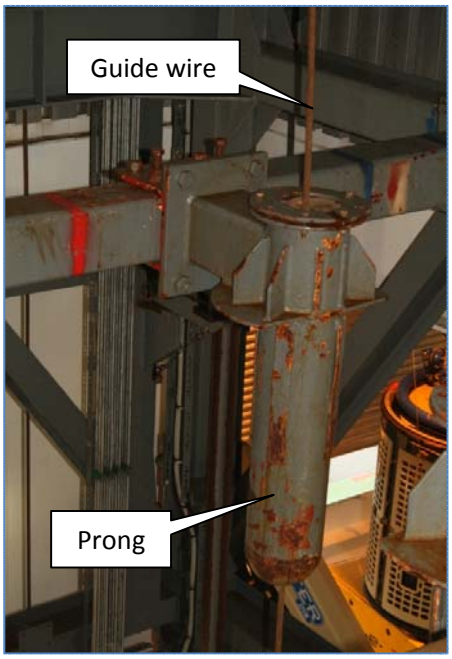

Figure 2.11 Havila Subsea prong

2.3.2.4 Skidding System

The skidding system is consisting of skidding tracks and skidding pallets, see Figure 2.12. The subsea equipment are transported from there storage locations and into the MHS area on special skidding pallets before they are hoisted into the sea.

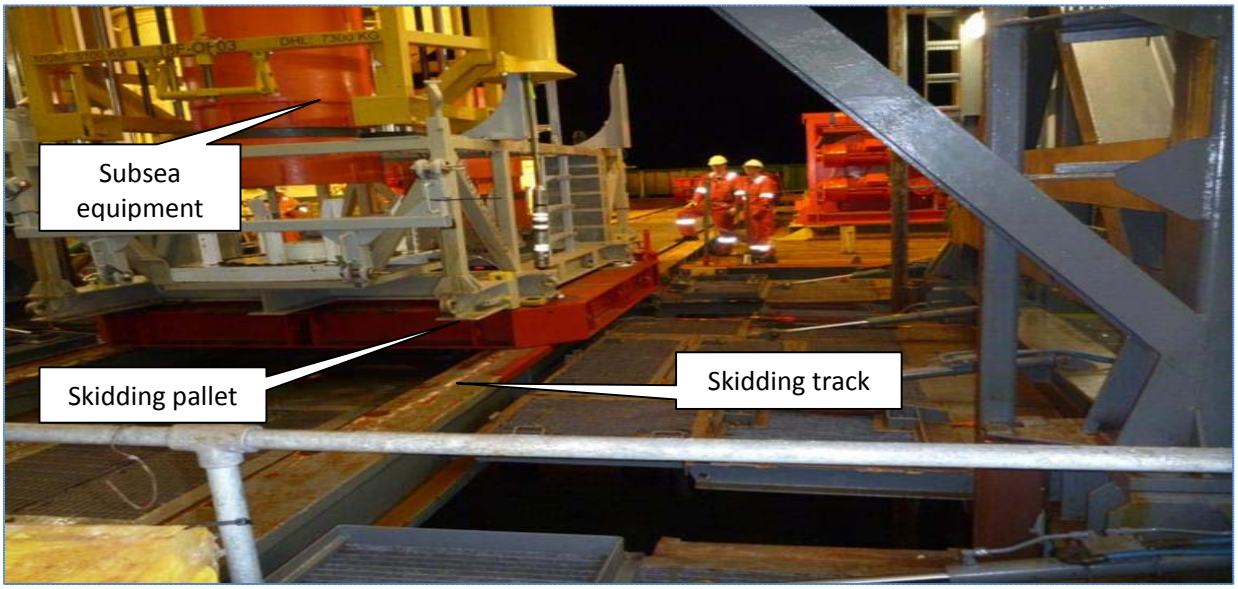

Figure 2.12 Skidding of Subsea equipment inside moonpool area on Havila Subsea (Heng, 2012)

On Havila Subsea, hydraulic jacks are pushing the pallets into desired location. The speed of these jacks is of concern and can, if increased, improve the vessel efficiency.

2.3.2.5 Main crane

The Havila Subsea main crane is used when lifting through the moonpool. The crane is a separate part of the MHS. The reason for not having a MHS lifting crane/winch is to save costs and weight. The crane has a lifting capacity of 150Te and is equipped with a Cranemaster heave compensating system.

2.3.3 Water kinematics

2.3.3.1 Inside moonpool

When an object is located inside the moonpool, only vertical water motions are considered. This consideration is valid due to the moonpool location (close to centre of pitch and roll) and the horizontal restrictions caused by the CF. Vertical water motions in moonpool can in general occur in two different situations:

- When the vessel is moving with forward speed.
- When the vessel is operation stationary with the influence of waves.

This thesis is emphasizing on moonpool operations during stationary conditions, thus water motions due to forward speed is neglected. Figure 2.13 shows how a vessel in stationary heave condition will be affected by the waves.

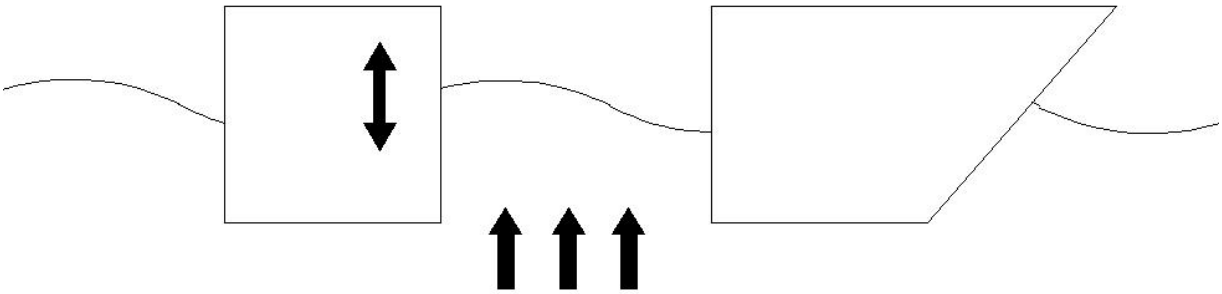

Figure 2.13 Vessel motions in stationary heave conditions

When the water particle inside the moonpool gets into resonance with the moonpool walls, we can experience large water plugs shooting up, these plugs are referred to as piston mode in the literature (Gaillarde and Cotteleer, 2004). Piston mode can result in large forces on equipment inside the moonpool and flooding of the moonpool area. This presents a hazard for crew and the stability of the vessel. Conditions with piston mode in the moonpool should always be avoided, but as the following calculations will show, this is not easy for Havila Subsea when operating in the North Sea.

The moonpool on Havila Subsea have a constant moonpool area, the dimensions are 7.2 m x 7.2 m. Because of this constant cross sectional area we can apply a simplified equation for calculating the moonpool resonance period (DNV, 2011b).

$$T(D) = \frac{2\pi}{\sqrt{g}}\sqrt{D + \kappa\sqrt{A}} \quad [\text{s}] \tag{2.5}$$

where:

$T(D)$ $= Moonpool\ resonance\ period\ [s]$
D $= Draft\ [m]$
κ $=$ Geometry factor $[-]$
A $= moonpool\ cross\ section\ area\ [m^2]$
g $= gravity\ constant\ [m/s^2]$

If the moonpool does not have a constant cross sectional area, reference is given to section 3.5.4.6 in DNV – RP – H103.

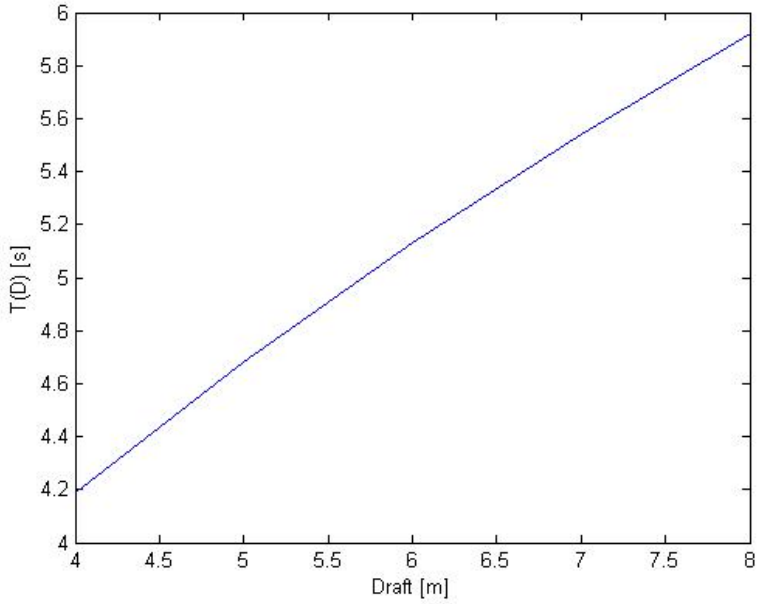

Figure 2.14 Havila Subsea moonpool resonance period as a function of the vessel draft

We see that Havila Subsea moonpool has a resonance period between 4.2 and 5.9 seconds. If we have in mind the equation for wave period (wave period = 2π/wave frequency) and compare with the JONSWAP spectrum, we see that Havila Subsea will most likely experience resonance conditions during operations in the North Sea (Stald, 2011). Figure 2.15 shows the JONSWAP spectrum.

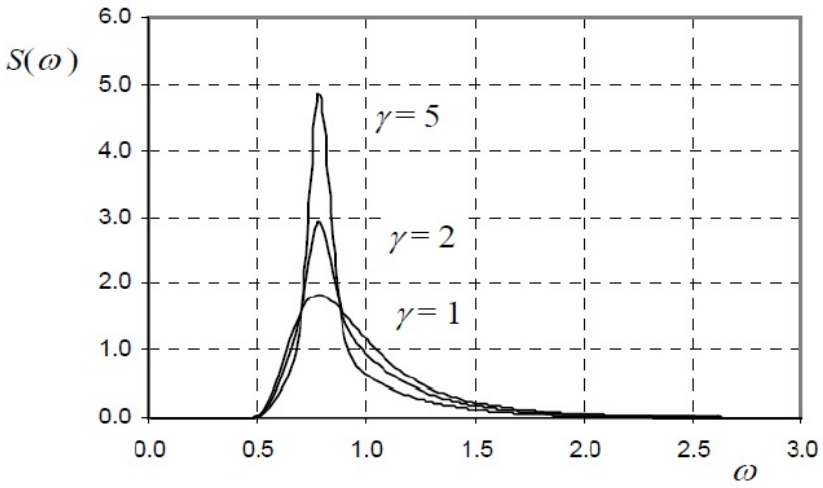

Figure 2.15 JONSWAP spectrum for Hs = 4,0m, Tp = 8,0 s for γ = 1, γ = 2 and γ =5

The JONSWAP spectrum gives us at which wave frequency we find the highest wave energy. The peak enhancement factor gamma (Ɣ) is used to take into account the fetch limited wind sea. The higher the peak factor is, the ``younger`` the sea-state is. Gamma = 1 represents a fully developed sea-state.

2.3.3.2 Outside moonpool

When large RTs are docked at the CF, the docking needs to take place outside the moonpool (underneath the vessel keel). During such a docking, large horizontal hydrodynamic forces are subjected to the RT. As a result, large forces on the prong tip will be experienced. Combined with the vessel rotational motions, these forces is the limiting situation for a moonpool lifting operation. Figure 2.16 illustrates the situation.

Side view

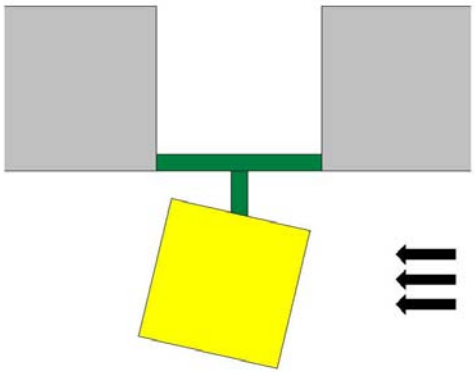

Figure 2.16 Hydrodynamic forces acting on a running tool when located outside moonpool

In order to get knowledge about the forces acting on the RT, linear wave theory needs to be taken into account. Linear wave theory can, to a large extent, describe the induced motions and loads acting on an object. The particle velocity is especially important because of its high contribution to the forces acting on an object. A brief outline of the derived formula for horizontal particle velocity is presented (Gudmestad, 2011):

$$u = \frac{\zeta_0 kg}{\omega} \sin(\omega t - kx) \quad [m/s] \tag{2.6}$$

where:

ζ_0 $= wave\ amplitude\ [m]$
g $= gravity\ constant\ [m/s^2]$
ω $= angular\ frequency\ [rad/s]$
$\omega = \frac{2\pi}{T}$

T $= wave\ period\ [s]$
k $= angular\ wave\ number\ [rad/m]$
$k = \frac{2\pi}{L}$

L $= wave\ length\ [m]$
t $= time\ [s]$
x $= direction\ of\ propagation\ [-]$

The vertical particle velocity presented here can only be applied for shallow water. This means when the water depth – wave length ratio is less than 0.05 ($\frac{d}{L} < \frac{1}{20}$). For other water depths, different formulas apply, reference is given to detailed linear wave theory.

2.4 Havila Subsea - moonpool handling procedures

The purpose of this subchapter is to give a general understanding of how the MHS on Havila Subsea is operated during an offshore operation.

2.4.1 Deployment

Installations of the subsea guidepost are the first task that is performed when Havila Subsea arrives on location. The guide posts are connection points for the guide wire at seabed. Havila Subsea is obliged to offset (10% of water depth) during the guidepost installation, this is to minimize the risk of dropt object damaging any subsea assets. When all guide posts are connected, the deployment procedure can commence.

Havila Subsea needs to orientate a suitable heading for deployment, heading directly towards the waves is common. When correct heading is achieved, the RT can be skidded into to moonpool area, see Figure 2.17. At the same time as the RT gets skidded into the moonpool area, the crane positions its tip directly above the moonpool.

Figure 2.17 Skidding of subsea equipment (Heng, 2012)

When the RT is placed inside the moonpool area, the rigging and main wire can be connected to the RT. The CF will be positioned directly over the RT, this is to align the RT funnels and CF prongs. When the rigging is complete, the RT can get disconnected from the skidding pallet. This gives clearance for the RT to be lifted of the skidding pallet and the pallet can be removed from the moonpool area, for safety reasons the crane is now set in locked mode. Before the hatches can get opened, the vessel needs to offset once again. The hatches needs to be opened manually one by one, this is a time consuming procedure, see Figure 2.18. The only hatch that is controlled hydraulically is the center hatch (skidding track hatch). When the moonpool is fully opened, the guide wires can be deployed and attached to the

subsea structure. As soon as all the guide wires are connected, the RT can be deployed. The lowering speed of the RT is approximately 0.5 m/s.

Figure 2.18 Moonpool hatch opening on Havila Subsea (Heng, 2012)

The CF follows the RT through the spash zone, see figure Figure 2.19, and down to the vessel keel. As the RT continues through the water, the horizontal hydrodynamic forces are taken by the guide wires, this can in rough weather conditions be a limiting factor. When the RT is approximately 20 m above the subsea structure the lowering stops, this is to make sure that the subsea guide pins and RT funnels are aligned. When alignment is achieved, a soft landing with speed of 0.05m/s can be carried out.

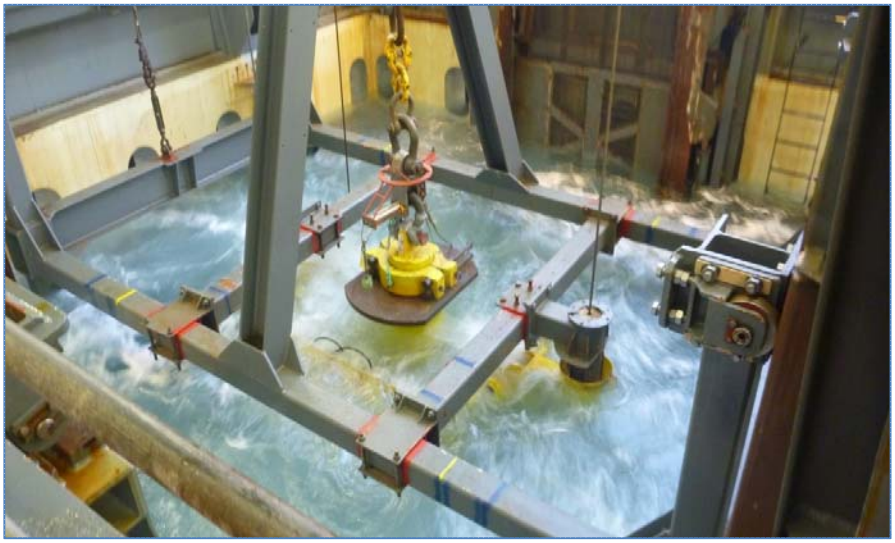

Figure 2.19 Subsea equipment getting lowered through moonpool splash zone (Heng, 2012)

2.4.2 Recovery

The recovery phase is performed as a reverse deployment. The critical part of the recovery phase is when the RT is docked onto Havila Subsea CF.

When the RT landed on the subsea structure, only the RT was moving. When docking onto the CF, both the RT and the vessel is moving, this generates large relative motions between the two and is the main limiting factor for MHS operations. In most operations the RT is docket inside the moonpool, this provides shelter against the hydrodynamic forces that are present outside the moonpool. However, large RTs can be docked underneath the keel, this is due to the small clearance between the RT and the moonpool walls. This type of docking can lead to large static and impulse loads on the prong. Figure 2.20 shows an illustration of FCMRT in the seconds before docking inside moonpool takes place.

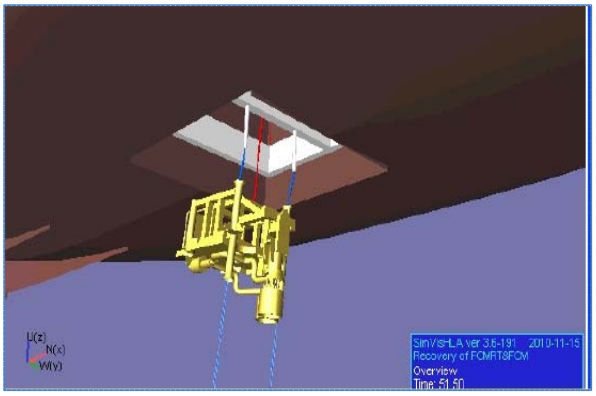

Figure 2.20 Docking of running tool inside moonpool (Acergy, 2010)

Another concern that is present when docking underneath the vessel is tilting. Since the vessel is orientated longitudinal against the waves, the RT will be exposed to large hydrodynamic forces in this direction. At the same time the vessel will surge, the combination of horizontal forces and vessel surge motion can cause the RT to start tilting. This tilting motion can in worst case cause the docking to fail. The titling motion is largest for the short wave periods. This is reasonable, since the RT follows the vessel motions for longer wave period (Acergy, 2010). Figure 2.21 illustrates how the FCMRT can tilt around the prongs.

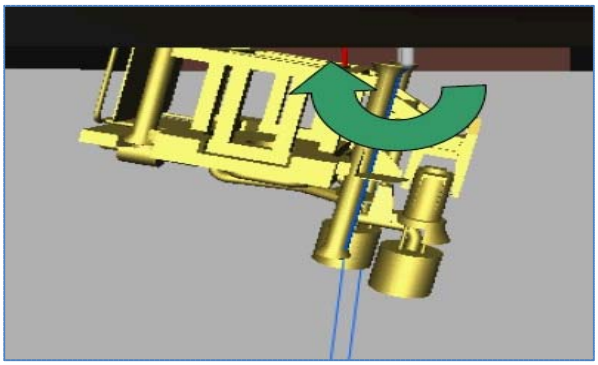

Figure 2.21 Running tool tilt around the prongs (Acergy, 2010)

Guide wire tension is an alternative that has been discussed in order to minimize the risk of tilting and impact loads between funnels and prongs. In general the docking will be smoother if the tension in the guide wire is increased. This seems reasonable as the guide wire will help the funnels onto the prong. However, analyses have shown that by increasing the guide wire tension, the RT can get stuck on the prongs. Hence, problems related to the docking of the RT onto the prong cannot in general be solved by simple increasing the guide wire tension (Acergy, 2010).

2.4.2.1 Weather limitations

Havila Subsea is like all other vessels restricted by weather conditions. For lifts through moonpool the wave height, H_s and the wave period T_p are important values. It has been shown (Acergy, 2010) that the wave period is the restricting factor with regards to loads on the prongs and CF. Even though this is not shown for Havila Subsea, the vessel configuration is fairly identical. Hence, it is reasonable to assume the same for Havila Subsea.

Which environmental conditions that limit a moonpool operation on Havila Subsea are different for each tool. A MIT can be deployed safely in significant wave height of 5m while FCMRT can be limited by a 3m significant wave height. Figure 2.22 illustrates the loads between funnels and prongs in a single time domain docking phase for FCMRT&FCM. The peak loads seen on the figure is impulse loading between the RT and the prongs.

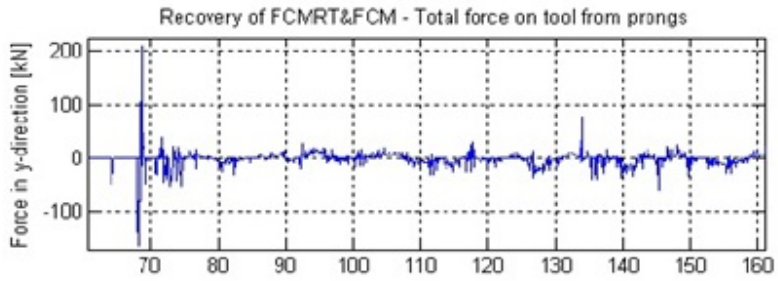

Figure 2.22 Recovery of FCMRT&FCM - Total force on tool from prongs (Acergy, 2010)

3 NEW SOLUTIONS, CALCULATIONS AND RESULTS

3.1 Chapter overview

This chapter presents the alternative prong design which has been discussed for improvement potential on Havila Subsea cursor frame. Structural analyses and results for capacity checks, cursor frame Staad.Pro analysis and force-deflection ratio for stiff and flexible prong are also presented and discussed.

3.2 Development of New prongs

Out of the three alternative prongs that are presented her, only one is chosen for improvement potential. This is the Vasshella SMART flexible prong, referred to as flexible prong in this thesis. The reason for choosing this solution for the improvement check is due to the progress of the development. The flexible prong has already been patented by Vasshella AS and a prototype is build. This prototype should have been tested during the work with this thesis. However, due to limited resources this has not been done. Only theoretical calculations have been performed.

3.2.1 Prong with Spring (PwS) – 1 of 3

PwS has a fairly simple design, here the flexibility is based on a spring section located at the middle of the prong. This type of design will give the possibility for the prong to take up loads in both horizontal and vertical direction without jeopardizing the structural integrity of the funnel or prong. Figure 3.1 shows a simple illustration of the conceptual design for the PwS. The basic idea behind the prong with spring is to provide a ``smooth`` docking of the RT funnels onto the CF prongs. The prong should be manufactured in steel, this is to keep the structural capacity as high as possible, and the prong should for simpler manufacturing and maintenance not include any moving parts.

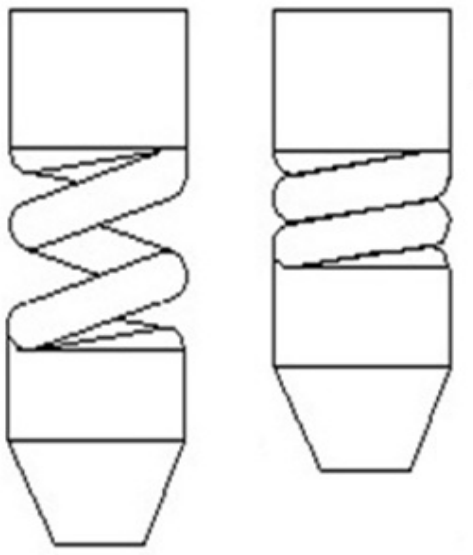

Figure 3.1 Prong with Spring

3.2.2 Prong with Neoprene (PwN) – 2 of 3

PwN is based on the idea that the prong is hollow and filled with a neoprene bearing, this is to take up the loads as the prong tip get pushed in the horizontal or vertical direction. See Figure 3.2 for illustration of the PwN.

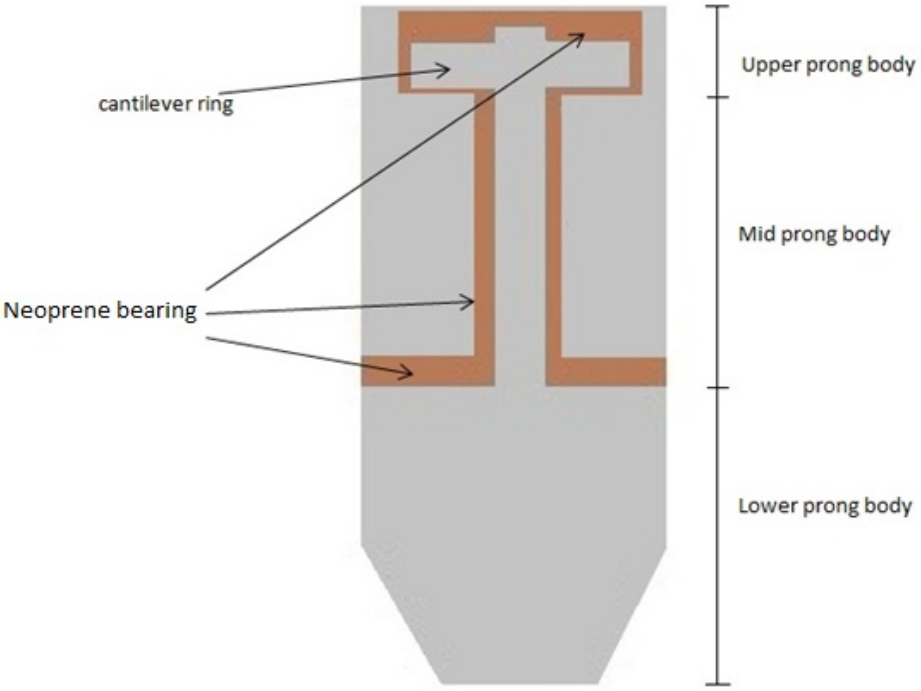

Figure 3.2 Prong with hollow section filled with neoprene bearing

As the illustration shows, the prong has been divided into three parts; upper, mid and lower prong body. The idea is that the lower part never should get into contact with the other prong body parts. The only interaction between the lower part and the two other should be through the neoprene bearing. The vertical part has a pole that runs through the mid part and up into the upper part. It's held in place in the vertical direction by a cantilever ring which is too big to pass through hole of the upper part of the prong body. Since the steel pole is completely covered with neoprene it will have flexibility in both horizontal and vertical direction. How much flexibility, will be decided by the elasticity of the neoprene. For this prong solution, the neoprene will be a critical element.

3.2.3 Smart Flexible Prong – 3 of 3

The Vasshella SMART flexible prong is based on the Vasshella Flexible Guide Post. The Flexible Guide Post is meant to cope with problems during Emergency Disconnect (EQD) of Lower Marine Riser Package (LMRP).

The flexible prong can provide an angular deflection of desired magnitude. For use in Havila Subsea MHS a maximum deflection of 5 degree should be sufficient. The deflection comes from a joint located at the upper part of the prong. When maximum deflection is reached, there will be steel on steel interface and the deflection stops. At maximum deflection a normal elasticity modulus for steel will apply.

The flexible element consists of rubber with several stainless steel plates vulcanized together in a mould. Pre tension of the rubber element will provide a higher initial stiffness of the prong. A typical stiffness for the element is 5 kNm (Pettersen, 2012).

The reason for using a SMART flexible prong is to minimize the risk of unwanted events. Such events can be fatigue in the CF, failed docking and large impulse loading. The SMART flexible prong can provide a safer and smoother docking than what is possible for stiff prongs.

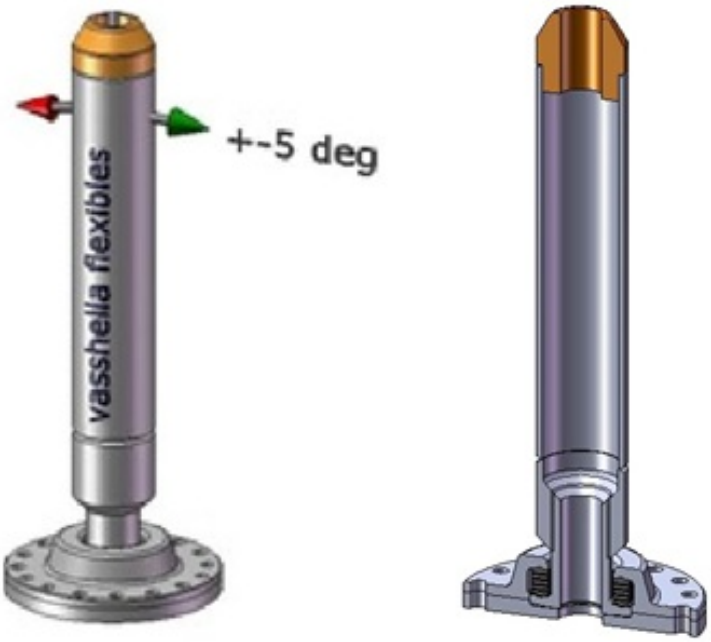

Figure 3.3 Smart flexible prong - Deflection and section view

3.3 Main calculations and results

Havila Subsea CF has been structural analyzed using hand calculations and the structural software Staad.Pro. The loads used in Staad.Pro have been found by using capacity check for the prong, CF connection beam, bolts and welds. All the capacities are according to NS3472 and can be seen in Appendix I.

Figure 3.4 Havila Subsea cursor frame - 3D model

Figure 3.4 show a 3D AutoCAD drawing of Havila Subsea CF. However there is one important difference between the AutoCAD drawing and the real CF. The drawing does not contain the connection beams between the prong and the cursor beam. As the calculations in this chapter will show, these connection beams are of high importance. Figure 3.5 shows a picture of the Havila Subsea CF, here the connection beams are easy to see.

Figure 3.5 Havila Subsea cursor frame - real view

3.3.1 Objective

The reason for performing a structural analysis of the CF is to:

- Find the weakest member of existing cursor frame (hand calculations)
- Find and investigate the existing capacities for the cursor frame (Staad.Pro)
- Check the force-deflection ratio for stiff and flexible prong (Staad.Pro)

In all the analyses the load is modeled to be static load acting on the prong tip. The reason for this is that Acergy running tool re-rating study indentified the following situation as governing:

The governing situation is large relative motions just when the tip of the prong are at the top of the funnel (Acergy, 2010).

3.3.2 Hand calculations

The loads which are used in the Staad.Pro analysis is found in a capacity check of the CF. The capacity check has been performed as a ``weak member`` analysis. The prong, cursor beam, connection beam, bolts and welds have been checked for capacities, these capacities have been converted into static loads on the prong. The lowest capacity was used as the highest load on the prong when analyzing in Staad.Pro.

When converting the capacities into static prong loads, structural mechanics calculations have been performed. This chapter will give an overview of how the formulas which are used when converting the capacities into static loads are calculated. Detailed capacity calculations and conversions into static prong load are presented in Appendix I.

Figure 3.6 illustrates the **cursor beam**, **connection beam** and **prong**.

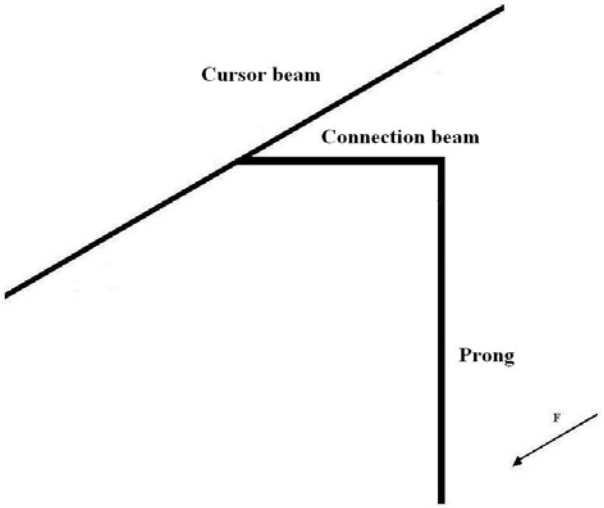

Figure 3.6 Cursor beam, connection beam and prong illustration

3.3.2.1 Prong

When we have a fully fixed cantilever beam we will experience bending moment and shear forces, these are expressed as:

$$Moment \qquad M = F \times L_p$$

$$Shear\ force \qquad V = F$$

where $\boldsymbol{F}$ is the static prong load, $\boldsymbol{L_p}$ is the length of the prong, $\boldsymbol{M}$ is the maximum prong moment and $\boldsymbol{V}$ is the prong shear force. This gives us the following static load formulas:

$$From\ moment \qquad F = \frac{M}{L_p}$$

$$From\ shear\ force \qquad F = V$$

3.3.2.2 Connection beam

The connection beam will experience moment, shear force and torsion. These forces are expressed as:

$$Moment \qquad M = F \times L_b$$

$$Shear\ force \qquad V = F$$

$$Torsion \qquad T = F \times L_p$$

where $\boldsymbol{F}$ is the static prong load, $\boldsymbol{L_p}$ is the length of the prong, $\boldsymbol{L_b}$ is the length of the connection beam, $\boldsymbol{M}$ is the maximum beam moment and $\boldsymbol{V}$ is the beam shear force. This gives us the following static load formulas:

$$From\ moment \qquad F = \frac{M}{L_b}$$

$$From\ shear\ force \qquad F = V$$

$$From\ torsion \qquad F = \frac{T}{L_p}$$

3.3.2.3 Cursor beam

The cursor beam is experiencing a more complex load distribution than the connection beam and prong. Because of the assumption that the beam is fully fixed at both ends, the cursor beam needs to be calculated as a statically indeterminate beam. This gives a somewhat more complicated calculation to find the end reactions and end moments.

The moment experience at the point where the prong is connected is possible to find without calculating the statically indeterminate beam. This is because of continuity in the beam. We know that when a moment is imposed onto a beam, half of this moment will be taken into the beam in negative and positive direction. See Figure 3.7.

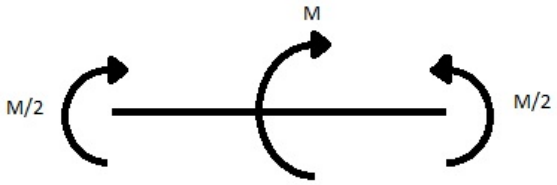

Figure 3.7 Moment continuity

This gives us the static load formula for the point where the prong is connected:

$From\ moment \qquad F = \frac{M \times 2}{L_p}$

$From\ axial\ force \qquad F = N$

It is common procedure to exclude the axial force in the simplified hand calculation. The end reactions and moment are used to check the cursor beam bolt and weld utilization.

The cursor beam can be illustrated as a fully fixed beam with a concentrated moment, see Figure 3.8:

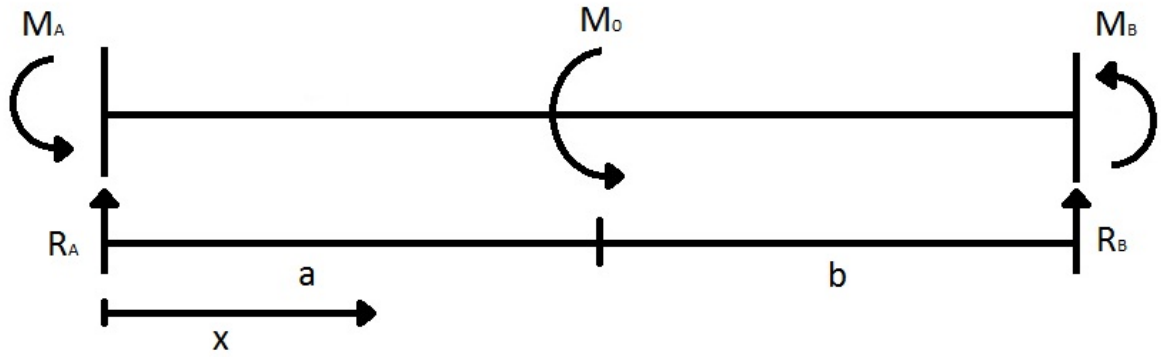

Figure 3.8 Cursor beam illustrated as a fully fixed beam with a concentrated moment

Static equilibrium for the whole cursor beam:

$R_A + R_B = 0$

$\rightarrow \qquad R_B = -R_A$

$M_A + M_B + M_0 - R_A L = 0$

$\rightarrow \qquad M_B = R_A L - M_0 - M_A$

The analyses start with considering equilibrium of the left part of the beam, the part left of the moment M_0.

$\boldsymbol{0 \leq x \leq a}$

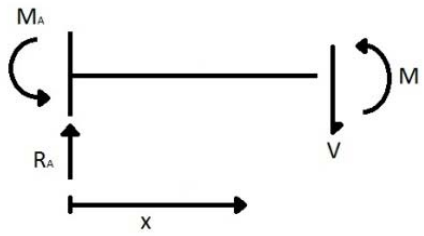

Figure 3.9 Right side of cursor beam

$R_A - V = 0$

$\rightarrow \quad R_A = V$

$M_A + M_0 - Vx = 0$

$\rightarrow \quad M_0 = -M_A + Vx = -M_A + R_A x$

$y_1'' = \frac{1}{EI}[-M_A + R_A x]$

$y_1' = \frac{1}{EI}\left[-M_A x + \frac{R_A}{2}x^2 + C\right] \qquad C = 0 \; as \; (y_1''(0) = 0)$

$y_1 = \frac{1}{EI}\left[-\frac{M_A}{2}x^2 + \frac{R_A}{6}x^3 + C\right] \qquad C = 0 \; as \; (y_1(0) = 0)$

$y_1'' = \frac{M}{EI}$ is called; *beam differential equation*. Here, this equation has been used to utilize the known boundary conditions for deflection (y_1).

The right side of the cursor beam also needs to be considered in a stat of equilibrium.

$\boldsymbol{a \leq x \leq b}$

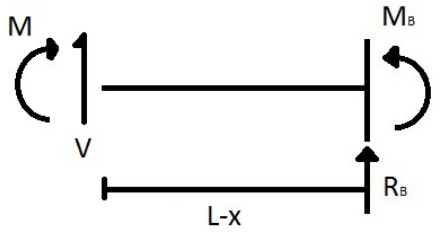

Figure 3.10 Left side of cursor beam

$R_B + V = 0$

$\rightarrow \quad V = -R_B$

$M_B - M_0 + R_B(L-x) = 0$

$\rightarrow \quad M_0 = M_B + R_B(L-x)$

$y_2'' = \frac{1}{EI}[M_B + R_B(L-x)]$

$y_2' = \frac{1}{EI}\left[M_B - R_B\frac{(L-x)^2}{2} + C\right] \qquad C = -M_B L \ as \ (y_2'(L) = 0)$

$y_2' = \frac{1}{EI}\left[-M_B(L-x) - R_B\frac{(L-x)^2}{2}\right]$

$y_2 = \frac{1}{EI}\left[M_B\frac{(L-x)^2}{2} + R_B\frac{(L-x)^3}{6} + C\right] \qquad C = 0 \ as \ (y_1(L) = 0)$

We now have the equilibrium equations for shear force, moment and deflection for both sides of the cursor beam. In order to find the equations for end reactions and end moments we need to use known boundary conditions. One boundary condition we can apply is; $y_1(a) = y_2(a)$. This gives that; $y_1'(a) = y_2'(a)$.

$y_1'(a) = y_2'(a)$

$\rightarrow \quad -M_A a + \frac{R_A}{2}a^2 = -M_B(L-a) - R_B\frac{(L-a)^2}{2}$ (1)

$y_1(a) = y_2(a)$

$\rightarrow \quad -\frac{M_A}{2}a^2 + \frac{R_A}{6}a^3 = M_B\frac{(L-a)^2}{2} + R_B\frac{(L-a)^3}{6}$ (2)

Now we need to use the initial equilibrium equations for the whole cursor beam in order to solve (1) and (2).

Initial equilibrium equations:

$R_B = -R_A$ (3)

$M_B = R_A L - M_0 - M_A$ (4)

It is also important to have in mind that; $L = a + b$

Substituting (3) and (4) into (1) and (2):

$$(1) \rightarrow \quad -M_A a + \frac{R_A}{2}a^2 = -(R_A L - M_0 - M_A)(L-a) + R_A \frac{(L-a)^2}{2}$$

$$\rightarrow \quad M_A = \frac{R_A L}{2} - M_0 \frac{(L-a)}{L} \qquad (5)$$

$$(2) \rightarrow \quad -\frac{M_A}{2}a^2 + \frac{R_A}{6}a^3 = (R_A L - M_0 - M_A)\frac{(L-a)^2}{2} - R_A \frac{(L-a)^3}{6}$$

$$\rightarrow \quad M_A L\left(\frac{L}{2} - a\right) = R_A\left(\frac{L^3}{3} - \frac{aL^3}{2}\right) - M_0 \frac{(L-a)^2}{2} \qquad (6)$$

we are left with two equations and two unknown, this is solved by substituting equation (5) into equation (6):

$$\left(\frac{R_A L}{2} - M_0 \frac{(L-a)}{L}\right) L\left(\frac{L}{2} - a\right) = R_A\left(\frac{L^3}{3} - \frac{aL^3}{2}\right) - M_0 \frac{(L-a)^2}{2}$$

We have now only one unknown, R_A.

$$\text{Solve for } R_A \rightarrow \quad R_A = \frac{6M_0 ab}{L^3} \qquad (3.1)$$

We now have everything we need to derive equations for R_B, M_A and M_B.

$$(3) \rightarrow R_B = -\frac{6M_0 ab}{L^3} \qquad (3.2)$$

$$(5) \rightarrow M_A = \frac{M_0 b}{L^2}(2a - b) \qquad (3.3)$$

$$(4) \rightarrow M_B = \frac{M_0 a}{L^2}(2b - a) \qquad (3.4)$$

These beam equations (3.1, 3.2, 3.3 and 3.4) are used for three different purposes in the analysis;

1. Finding out the moment and shear distribution across the cursor beam
2. Finding the worst location for the prong with regards to bending moment in the cursor beam
3. Checking utilization for bolt and welds at the cursor beam ends

Number 2 and 3 are not shown in this chapter, they are presented in Appendix I.

Figure 3.11 shows a MATLAB plot of the cursor beam shear force and bending moment diagram when an 112kNm moment is applied to the middle of the cursor beam.

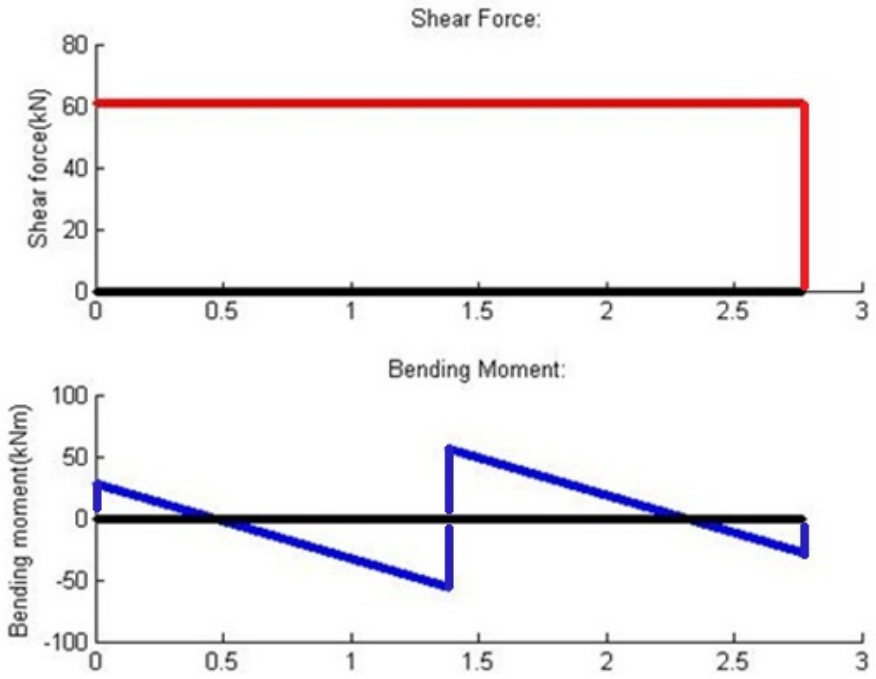

Figure 3.11 Cursor beam shear and moment distribution when concentrated moment is applied

The capacity calculations show that the member with lowest capacity is the prong. Table 3-1 shows the different cursor frame capacities. Detailed capacity calculations are found in Appendix I.

Table 3-1 Cursor frame capacities

Member	Length [m]	Max tip Load [Te]	Reason for yield
Prong	0.9	11.86	bending
Connection beam	0.2	14.4	Reduced bending capacity due to torsion
Cursor beam	2.77	32.3	bending
Bolts	-	97.66	Bolt hole pressure
Weld	-	12.96	Shear and bending

3.3.3 Staad.Pro analysis of cursor frame

This chapter presents the Staad.Pro structural analysis of the CF. Even though the capacity calculations have shown the prong to be the weakest member, it is important to check the load distribution for different cursor beam and prong setups. As mentioned in chapter 2.3.2.3.2, the CF and the prong locations are depending on the RT size and geometry. Hence, the load distribution across the cursor frame is constantly changing.

Cursor frame materials (S355):

Yield strength:	f_y = 355 N/mm^2
Tensile strength:	f_u = 510 N/mm^2

Defaults value in Staad.Pro for steel materials:

Young's modulus:	E = 205 N/mm^2
Steel density:	ρ = 7700 kg/m^3
Poisson number:	ν = 0.3

Figure 3.12 shows a 3D rendering model of the CF in Staad.Pro.

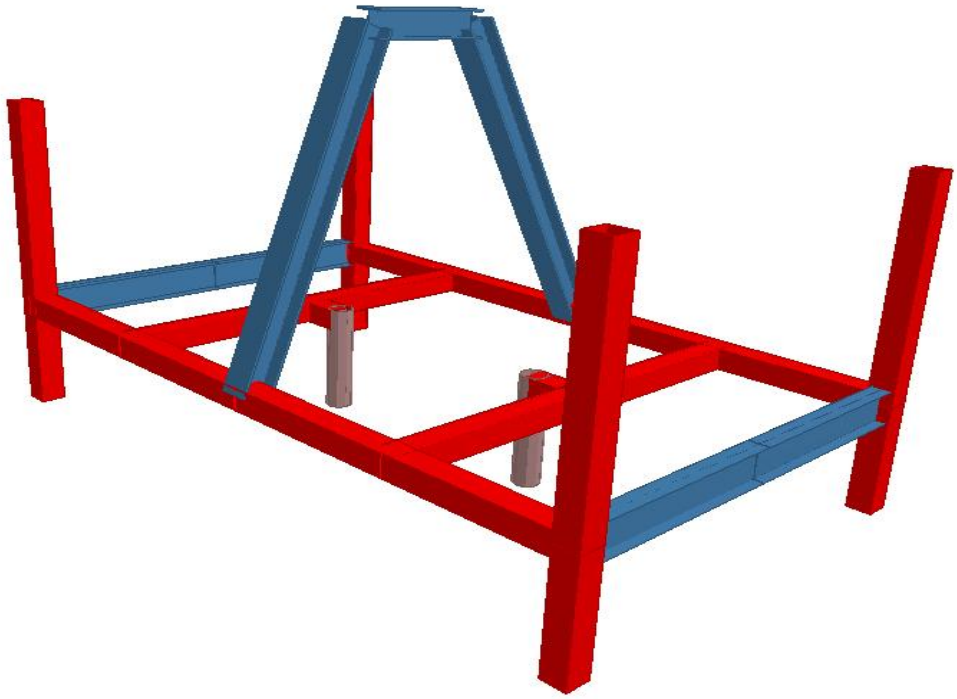

Figure 3.12 Staad.Pro 3D rendering model of Havila Subsea cursor frame

Eight separate CF models have been analyzed in Staad.Pro. All the models had different cursor beam and prong location. The loads applied in the models are 116 kN and is applied in two different directions. These directions are representing longitudinal force (F_x) and transverse force (F_y). F_x is the prevailing force direction for moonpool operations through moonpool.

Only results from two of the eight models are presented in this chapter, this is model 1 of 8 and 7 of 8. The reason for this is that seven of the models showed a fairly identical load distribution across the CF. The only model which showed any difference is model 7.

Figure 3.13 show the different load directions and the member numbering system for the highest utilized members. Beam 5, 6 11 and 12 are referred to as the CF side beams in this thesis.

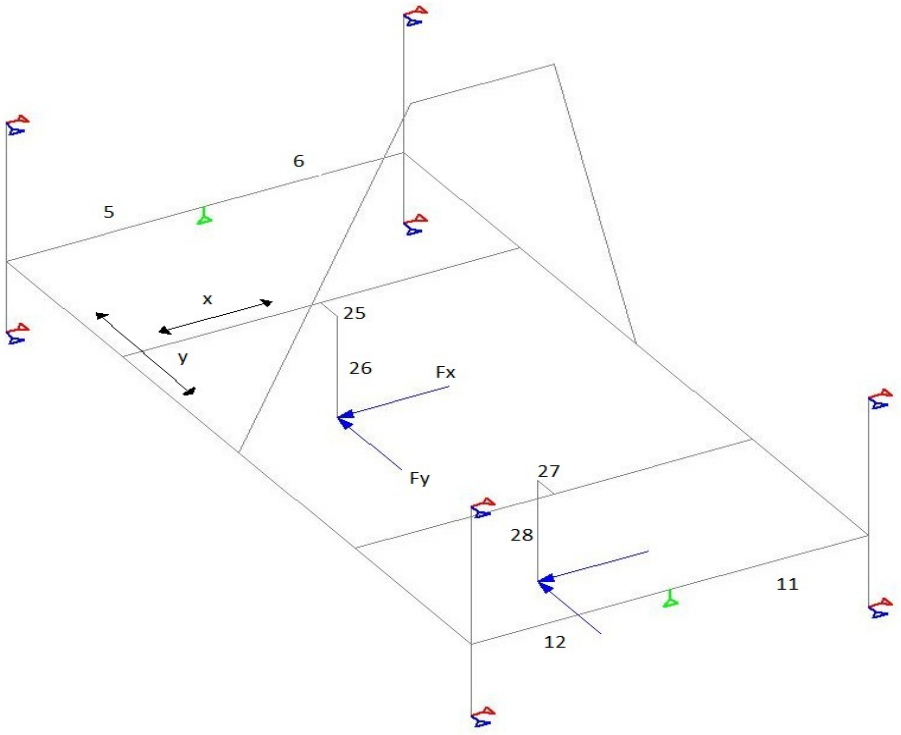

Figure 3.13 Cursor frame load directions and numbering system

In the first five models, the prongs were moved in the **x-direction**, along the cursor beam. In the three last models the prongs were placed in the middle of the cursor beam and the cursor beams were moved in the **y-direction**, along the length of the CF.

3.3.3.1 Load setup 1 of 8:

Load setup 1 represents a symmetric CF configuration. The prongs are placed in the middle of the cursor beam and the cursor beam is placed in the middle of the transverse CF beams.
Figure 3.14 shows the members with highest utilization.

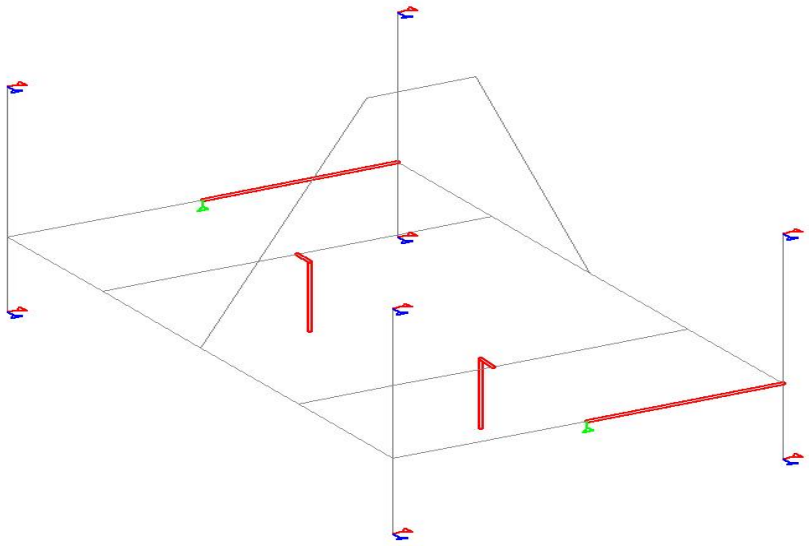

Figure 3.14 Load setup 1 of 8 - highest member utilization

Table 3-2 Load setup 1 of 8

Member	Mean US	US	Clause	Force direction
26	0.436	1	von Mises	Fx and Fy
28		1	von Mises	Fx and Fy
25		0.944	von Mises	Fx
27		0.944	von Mises	Fx
6		0.859	von Mises	Fx
11		0.859	von Mises	Fx

As expected the load distribution across the CF is symmetrical. The prongs are the weakest members. We see that the prevailing force direction, Fx, is the dimensioning force direction for the CF.

3.3.3.2 Load setup 7 of 8:

Load setup 7 represent a load setup where the prongs are placed in the middle of the cursor beam and the cursor beams are placed very close to the main wire, 1 m apart. This CF configuration is valid for small RTs or RTs with funnels placed close together. Figure 3.15 shows the members with the highest utilization.

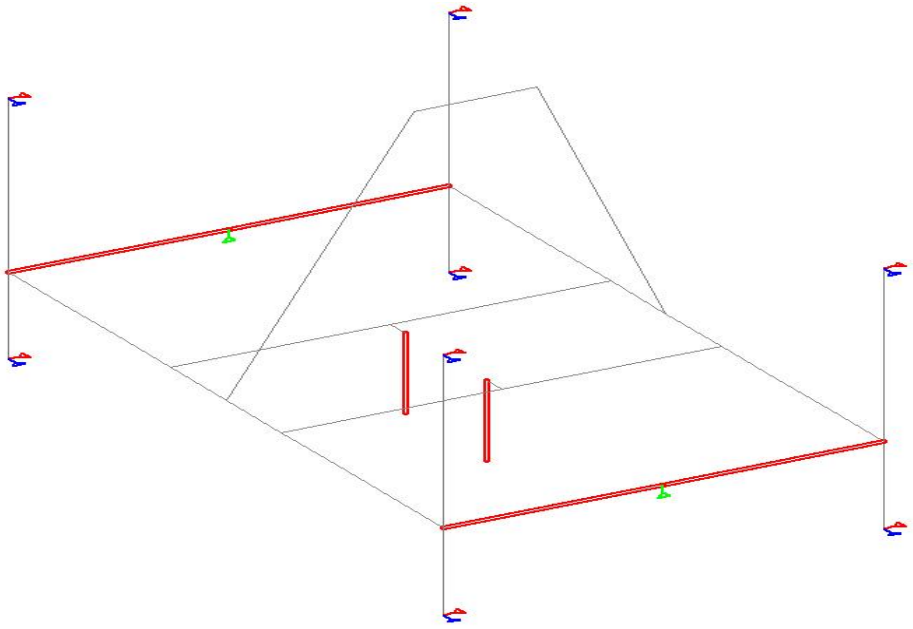

Figure 3.15 Load setup 7 of 8 - highest member utilization

Table 3-3 Load setup 7 of 8

Member	Mean US	US	Clause	Force direction
6	0.609	1.33	von Mises	Fx
11		1.33	von Mises	Fx
5		1.29	von Mises	Fx
12		1.29	von Mises	Fx
26		1	von Mises	Fx and Fy
28		1	von Mises	Fx and Fy

For load setup 7 something interesting was found. The prongs are not longer the weakest member, for this CF configuration the CF side beams are yielding at a lower load than the prongs. This is important for operations where small RTs or RTs with funnels close together are used. This CF configuration also shows a higher mean utilization for the entire cursor frame. This can be explained as a consequence of the large moment arm generated on the CF side beams when loads are applied close to the CF centre of gravity.

3.3.4 Staad.Pro analysis of existing and alternative prong

The cursor beam analysis is performed to find the force-deflection ratio of the existing and alternative prong. The alternative, flexible prong has been modeled with a lower elasticity modulus (E) in the upper 10 cm than the stiff prong. This is to imitate the flexible element in the Vasshella flexible prong. The rest of the prong length has a normal, steel E-modulus (205 GPa). In order to get a realistic stiffness of the flexible prong, a dynamic stiffness should have been implemented in the model. Dynamic stiffness means that the resistance against bending the prong will increase linear with the angular deflection. Due to limitations in Staad.Pro and time constrains of this thesis, a dynamic stiffness analysis has not been performed. Hence, the results are recommended to only be used as an indicator of how the flexible prong will behave during loading. Figure 3.16 shows an illustration of the cursor beam, connection beam and prong isolated from the rest of the CF.

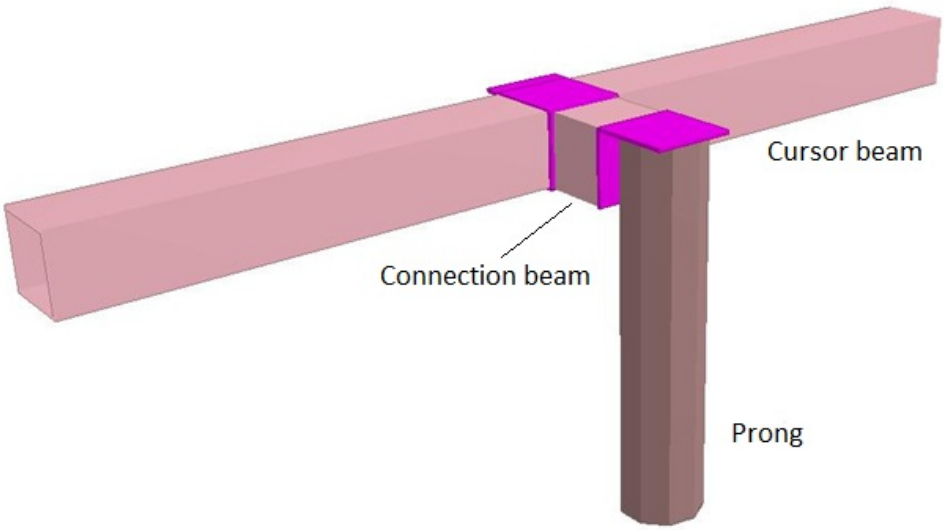

Figure 3.16 Staad.Pro model of cursor beam, connection beam and prong

The E-modulus which has been used to imitate the flexibility has been calculated using simple deflection formulas for a cantilever beam. Since the maximum prong angle is known to be 5 degrees and the length of the prong is 900 mm, a maximum deflection is calculated to be 78 mm. The force subjected to the prong when calculating the E-modulus, is the maximum yielding force found in the capacity check, 116 kN.

$$\delta = \frac{FL^3}{3EI} \tag{3.5}$$

$$\rightarrow \quad \mathrm{E} = \frac{FL^3}{3\delta I} \tag{3.6}$$

$$\rightarrow \quad \underline{E = 10058\ N/mm^2}$$

This is approximately 5% of the stiff prong elasticity.
In the analysis, loads from 80 to 116 kN is subjected to the prong tip. The difference in deflection is presented is Figure 3.17.

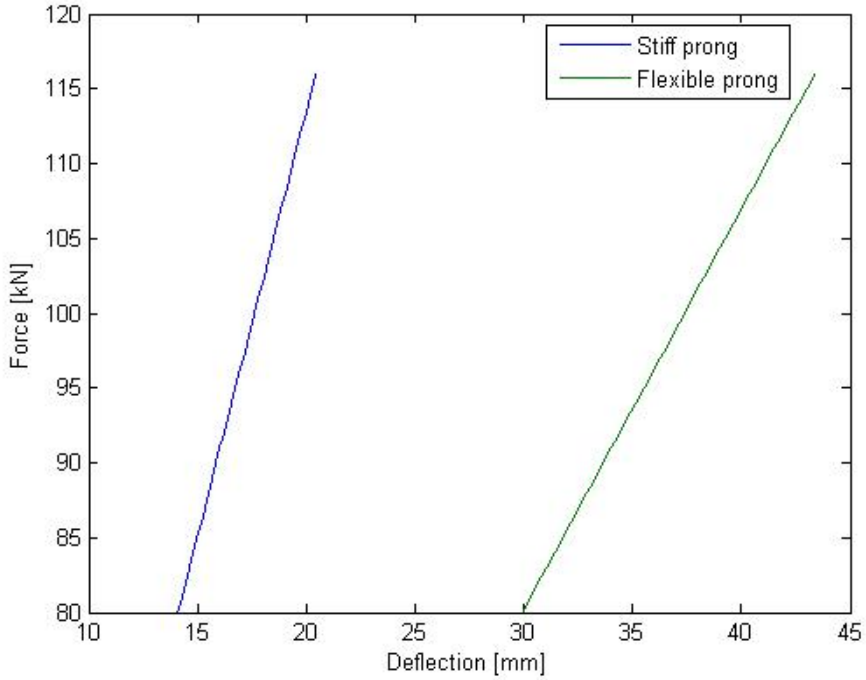

Figure 3.17 Force VS deflection for stiff and flexible prong

As expected these graphs show a higher deflection for the flexible prong. However, the force – deflection ratio for the flexible prong is show to be higher than for the stiff prong.

The force-deflection ratio is primarily meant to be used for realistic RT docking simulations, in the time domain simulation software SIMO. However, the results can also say something about the benefits of flexible prongs. Decreased stiffness means a larger time interval before the deflection stops. This means larger amounts of energy used for deflection and less used for structural stress in the prong. Because of this it is reasonable to say that the impulse load behavior is far more beneficial for the flexible prong than for the stiff one.

4 DISCUSSION

The issues discussed here are based on the calculated results and realizations made during the work of this thesis.

4.1 Cursor Frame

The results from the structural analysis have shown that the prongs are the weakest members in the cursor frame structure. The maximum static tip load per prong are 116 kN (11.86Te), this correspond to a vessel pitch angle of 34 degree, when both prongs are taking the load. Having in mind that at 10 degree pitching angle, most people are afraid the vessel is going to sink, 34 degree pitch is unrealistic. Even though the prong has been identified as the weakest member, there are other structural concerns to be aware of.

The connection beam is subjected to high torsion loads. Because of these loads the cross section shear flow is increased, as a consequence the connection beam yield strength is reduced, ref NS3472 ch.12.2.7 (Norsk Standard, 2001). In 2003 a series of full scale torsion tests on Rectangular Hollow Sections (RHS) was performed on The University of Nottingham. The tests consisted of comparing the torque twist behavior of RHS sections, thick wall theory, finite element analysis and full scale tests. For the elastic range, the experimental and the theoretical predictions did agree, but the tests showed a significantly lower torsion capacity than for those calculated (Ridley-Ellis et al., 2003). The report concluded with;

The disparity between the theoretical and measured torsional capacity is sufficiently large to cause concern, as it indicates that current design expressions overestimates the true capacity by around 15% (Ridley-Ellis et al., 2003).

If the torsion capacity is overestimated with 15%, the weakest member of the cursor frame can in reality be the connection beam. The total cursor frame capacity is then reduced to approximately 20.1 Te. This is a significant difference and can be a limiting factor for the operational sea state limits. Compared to the loads that are measured between the RT and prong today, 20.1 Te is more than enough. However, for future tool design this cursor frame weakness, needs to be taken into consideration.

Fatigue is not accounted for in the calculations, this can after some years of operation be important to check. The prongs and the cursor beam are subjected to cyclic hydrodynamic load during each deployment and recovery through moonpool.

When analyzing the whole cursor frame in Staad.Pro, the prong and the connection beam was shown to be the weakest members in most cursor frame setups. However, when the cursor beams were located close to the main wire, something interesting occurred. The prongs and connection beams were no longer the weakest members, as the cursor frame side beams started yielding at approximately 17% lower load than the prongs. This type of cursor frame setup can be valid for small types of RTs. Even though this was an interesting finding, it doesn't have much realistic value. This is because of the weight

of tools which need this type of cursor frame setup. As mentioned, this is a setup for small tools, and small tools often have low weight. Hence, the loads will most likely not reach the magnitude applied in the analysis. However, in a future perspective one never knows what kind of tools that can be designed and put into use.

4.2 Alternative - flexible prong

Impulse loading is something that is important when discussing sudden loads such as the funnels and prongs interactions. This is an issue that is very important if the new flexible Vasshella prong gets taken in use. In general the load distribution on the prong and cursor frame is the same as with a stiff prong. The difference is the change of quantity of motion. Docking onto stiff prongs vs. flexible prongs can in principle be compared to; jumping from ten feet onto concrete vs. grass, respectively. The total forces subjected to the body is the same, but the impulse loading is difference. An impulse subjected to a body is equal to the change in quantity of motion. Rouge, principle calculations(Appendix II), show that when applying a prong which can deflect 5 degrees in all directions, the impulse loading can get reduced by approximately 60%. Because of this it is reasonable to say that the impulse load behavior is far more beneficial for the flexible prong than for the stiff one.

Some advantages are also discovered for an operational point of view. If the vessel experiences large roll or pitch motions just as the RT funnels have started to dock onto the prongs, docking can fail due to stuck prongs or broken/over stressed guide wires. The flexible prongs will follow the vessel motion and therefore not creating any risk of stuck prong or over stressed guide wire before the vessel motion reaches 5 degrees. See Appendix IV for illustration.

4.3 Limitations

The complexity of the operational aspects regarding moonpool operations on Havila Subsea is very hard to model realistically in theoretical analysis. This is due to factors which play an important role with respect to handling of equipment on deck and the hydrodynamic aspects inside moonpool. In order to maximize the capabilities for the Havila Subsea MHS, logged data from an actual offshore operation should be gathered.

In the Staad.Pro analysis there can be some faults regarding the models. This is due to the sections and member available in the software. The Havila Subsea cursor frame has several plates and bolts which are not included in the model. This can give unrealistic utilizations and force distribution across the cursor frame.

Due to time constrain and resources available for this thesis, rough calculations have been performed for maximum pitch angle and impulse loading. The results from these calculations are not meant as ``real`` values, but as an indicator of principles.

5 CONCLUSION

On background of the results presented and discussed, the following conclusion may be drawn according to the scope of work for the thesis.

Given that the assumptions made and that the Staad.Pro model analyzed is correct, it is clear that the cursor frame on Havila Subsea have a high structural capacity. The prongs have been shown to be the overall weakest member in the cursor frame. Because of this it is conclusive to say that Havila Subsea cursor frame structural integrity is kept intact as the system is designed today. The loads seams not to be of any hazard to the cursor frame. However, the tools operated on Havila Subsea can have a lower structural capacity, hence; the tools can be subjected to loads higher than designed for.

Implementation for the Vasshella flexible prong will most likely have a beneficial effect. As discussed in this chapter 4, the flexible prong will have a better capability to handle large impulse loads and therefore be better with respect to fatigue. The flexible prong will also provide a smoother docking when large roll or pitch motions are made by the vessel.

The connection beam between the prong and the cursor beam has, because of torsion, been show to have an undetermined capacity. This leads to an uncertainty regarding the cursor frame capacity. This uncertainty can be eliminated with a new cursor frame design where the prong is connected directly to the cursor beam.

Personnel operation Havila Subsea MHS should have in mind that when changing the cursor beam and prong setup, the load distributions in the cursor frame also changes. This is especially important for heavy tools which have the funnels located near each other. In this situation it has been shown that the prong capacity is not longer of concern, the cursor frame side beams are the weakest members.

The skidding system is to slow. If the skidding pallets could be connected to some sort of winch inside the moonpool area the efficiency of deck handling would increase.

As for the skidding system the moonpool hatch system is to slow and complicated. In most vessels the moonpool is covered by 3 hatches, 2 side and 1 middle. On Havila Subsea there are 17 hatches and 16 of them needs to be opened manually. This is a time-demanding and hazardous procedure which should be improved. A 3 hatch hydraulically controlled system, should be installed, this would increase the efficiency for moonpool operations.

6 FURTHER WORK

The flexible prong can be modeled in ANSYS Classic in order to define a dynamic stiffness. This would give the possibility to simulate the RT docking phase in a more realistic manner than what is the case today. The stiffness can be modeled to change in time steps from the starting position until the deflection stops at 5 degree.

The cursor frame can be tested with tension-type load cells during an offshore operation. Preferably in harsh weather conditions when a heavy running tool is being operated. Alternatively, a scale model of the cursor frame could be made and tested.

Dynamic time domain calculation can be performed for the prong and cursor frame. These calculations can be used to check fatigue in the cursor frame members.

REFERENCES

ACERGY 2010. Acergy running tool re-rating study.
BENEDICT, H. K., BALDAUF, M. & KIRCHHOFF, M 2004. Estemating Potential Danger of Roll Resonance for Ship Operation. Hochshule Wismar - University of Technology, Business and Design; Dept. of Maritime Studies.
DNV 2011a. DNV-OS-H101, Marine Operations, General. Norway.
DNV 2011b. DNV Rules for Planning and Execution of Marine Operations, Ch: 4-5.
DNV 2011c. Modelling and analysis of marine operations. *DNV-RP-H103.*
FALTINSEN, O. M. 1990. Sea Loads on Ships and Offshore Structures. Cambridge: Cambridge University Press.
FMC. 2010. *Subsea to Beach Scenario* [Online]. Available: http://www.german-oilgas-expo.com/g-news-siemens-fmc-subsea-cooperation.htm [Accessed 14.04 2012].
GAILLARDE, G. & COTTELEER, A. 2004. Water motions in moonpools - Empirical and Theoretical approach.
GUDMESTAD, O. T. 2011. *RE: Lecture Notes in MOM480 - Marine Technology and Design.*
HENG, D. 2012. *RE: Personal communication with: Field engineer on Havila Subsea.*
NORSK STANDARD 2001. Steel Structures - Design Rules. *NS 3472.* Norway: Norsk Standard.
NPD. 2011. *Subsea Wells Produce most* [Online]. Stavanger. Available: http://www.npd.no/en/news/News/2011/Subsea-wells-produce-most/ [Accessed 17.01 2012].
PETTERSEN, E. 2012. *RE: Personal communication - Vasshella flexible prong.*
RIDLEY-ELLIS, D. J., OWEN, J. S. & DAVIES, G. 2003. Torsional behaviour of Rectangular Hollow Sections. School of Civil Engineering - The University of Nottingham, Nottingham, UK.
SCHJELDRUP, J. H. 2011. *RE: Havila Subsea - Moonpool Handling System.*
STALD, T. C. 2011. *Assessment of Critical factors when running and retrieving FRAMO pump modules through moonpool.* Master.
SUBSEA 7. 2011. *Subsea 7 vessel library* [Online]. Available: http://www.subsea7.com/fleet/vessels.html [Accessed 17.05 2012].

APPENDIX

Appendix I: **Cursor frame capacity – Hand calculations**

Appendix II: **Impulse load calculations – Stiff vs. flexible prong**

Appendix III: **Maximum pitch angle**

Appendix IV: **Flexible prongs following vessel motion**

Appendix I: Cursor frame capacity – Hand calculations

Calculations for prong, cursor beam, welds, plates and bolts.

Simplified illustration of the cursor beam and prong.

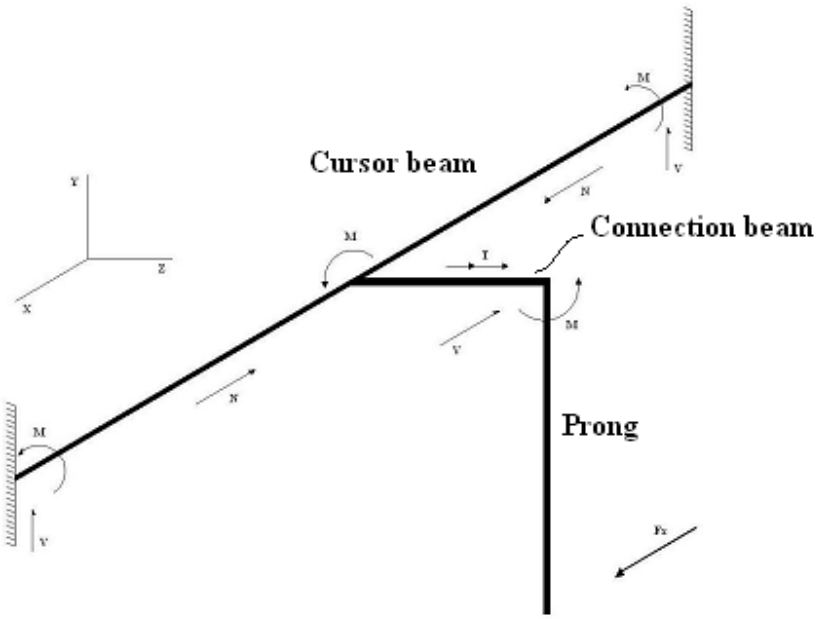

X is the prevailing load direction.

notation $_{p}$ means prong and notation $_{cb}$ means cursor beam and notation $_{co.b}$ means connection beam

Input data:

Material factor: $\gamma_{M1} := 1.1$

Material factor bolt: $\gamma_{M2} := 1.25$

Yield stress S355 steel: $f_y := 355MPa$

Prong input data:

Length of prong: $L_{prong} := 900mm$

Outer diameter of prong: $OD := 219mm$

Wall thickness of prong: $t_{w.p} := 10mm$

Inner diameter of prong $ID := OD - 2 \cdot t_{w.p}$

$ID = 199 \cdot mm$

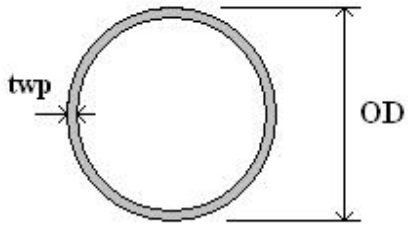

Cursor beam and connection beam input data:

Cursor beam heigth: $h_{cb} := 200mm$

Cursor beam width: $w_{cb} := 200mm$

Cursor beam wallthickness: $t_{w.cb} := 10mm$

Length of cursor beam: $L_{cb} := 2770mm$

Length of connection beam: $L_{co.b} := 200mm$

Max width to thickness ratio: $c_{cb} := h_{cb} - 2 \cdot t_{w.cb}$

$c_{cb} = 180 \cdot mm$

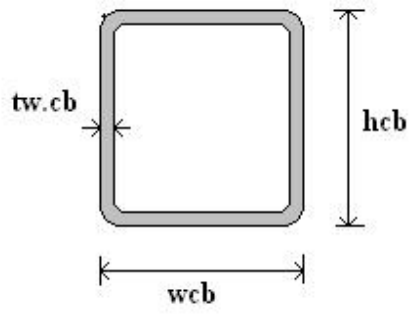

Prong position on the cursor beam:

$Length := 2770mm$

$a := 0mm, 1mm .. Length$

$b(a) := Length - a$

$M_0 := 10kNm$

$$M_{dist}(a) := M_0 \cdot \left[\frac{-6 \cdot a^2 \cdot b(a)}{Length^3} - \frac{b(a)}{Length^2} \cdot (Length - 3 \cdot a) + 1 \right]$$

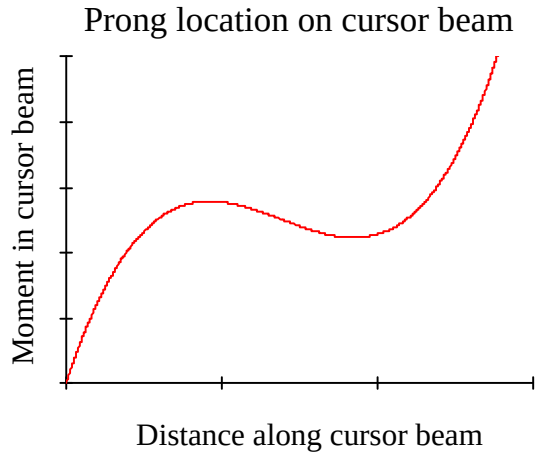

We can see here that the prong will give the highest bending moment if located at one end.

Prong calculations:

Yield ratio: $\varepsilon := 0.81$

Section class:

$$Class_{prong} := \begin{cases} "1" & \text{if } 0 \le \frac{OD}{t_{w.p}} \le 50 \cdot \varepsilon^2 \\ "2" & \text{if } 50 \cdot \varepsilon^2 \le \frac{OD}{t_{w.p}} \le 70 \cdot \varepsilon^2 \\ "3" & \text{if } 70 \cdot \varepsilon^2 \le \frac{OD}{t_{w.p}} \le 90 \cdot \varepsilon^2 \\ "4" & \text{otherwise} \end{cases}$$

$Class_{prong} = "1"$

Calculation of cross section properties:

Cross section area:

$$A_{pr} := \pi \cdot \left[\left(\frac{OD}{2} \right)^2 - \left(\frac{ID}{2} \right)^2 \right]$$

$$A_{pr} = 6.566 \times 10^3 \cdot mm^2$$

Moment of inertia:

$$I_{pr} := \frac{\pi}{4} \cdot \left[\left(\frac{OD}{2} \right)^4 - \left(\frac{ID}{2} \right)^4 \right]$$

$$I_{pr} = 3.593 \times 10^7 \cdot mm^4$$

Elastic section modulus:

$$W_{e.p} := \frac{I_{pr}}{\frac{OD}{2}}$$

$$W_{e.p} = 3.282 \times 10^5 \cdot mm^3$$

Plastic section modulus:

$$W_{pl.p} := \frac{4}{3} \cdot \left[\left(\frac{OD}{2} \right)^3 - \left(\frac{ID}{2} \right)^3 \right]$$

$$W_{pl.p} = 4.371 \times 10^5 \cdot mm^3$$

Moment capacity:

Plastic moment capacity:

$$M_{pl.Rd.p} := \frac{W_{pl.p} \cdot f_y}{\gamma_{M1}}$$

$$M_{pl.Rd.p} = 141.078 kNm$$

Elastic moment capacity:

$$M_{el.Rd.p} := \frac{W_{e.p} \cdot f_y}{\gamma_{M1}}$$

$$M_{el.Rd.p} = 105.904 kNm$$

Tip load due to moment capacity:

$$Tip_{mom.el.p} := \frac{M_{el.Rd.p}}{L_{prong}}$$

$$Tip_{mom.el.p} = 117.671 kN$$

Shear capacity:

Shear area: $A_{v.pr} := \frac{2}{\pi} \cdot A_{pr}$

$A_{v.pr} = 4.18 \times 10^{3} \cdot mm^{2}$

First moment of area: $S_z := \frac{W_{e.p}}{2}$

$S_z = 1.641 \times 10^{5} \cdot mm^{3}$

Plastic shear capacity: $V_{pl.cap.p} := \frac{f_y}{\gamma_{M1} \cdot \sqrt{3}} \cdot A_{v.pr}$

$V_{pl.cap.p} = 778.846\,kN$

Tip load due to shear capacity: $Tip_{sh.pl.p} := V_{pl.cap.p}$

$Tip_{sh.pl.p} = 778.846\,kN$

Reduction of moment capacity:

$\frac{Tip_{mom.el.p}}{Tip_{sh.pl.p}} = 0.151$ NO capacity reduction due to shear.

Elastic capacity check, von Mises:

Shear stress: $\tau_p := \frac{Tip_{mom.el.p}}{A_{v.pr}}$

$\tau_p = 28.151 \cdot MPa$

Bending stress:

$$\sigma_p := \frac{M_{el.Rd.p}}{I_{pr}} \cdot \frac{OD}{2}$$

$$\sigma_p = 322.727\,MPa$$

von Mises criteria:

$$\sigma_{j.p} := \sqrt{\sigma_p^{\,2} + 3 \cdot \tau_p^{\,2}}$$

$$\sigma_{j.p} = 326.39\,MPa$$

Elastic criteria:

$$\sigma_{d.p} := \frac{f_y}{\gamma_{M1}}$$

$$\sigma_{d.p} = 322.727\,MPa$$

We see that the von Mises criteria is **NOT** OK. This is due to the bending stress, hence the moment capacity needs to be reduced.

Maximum allowable bending stress:

$$\sigma_{p.max} := \sqrt{\sigma_{d.p}^{\,2} - 3 \cdot \tau_p^{\,2}}$$

$$\sigma_{p.max} = 319.023\,MPa$$

From the maximum allowable bending stress we can calculate the maximum allowable bending moment.

Maximum allowable bending moment:

$$M_{p.all} := \frac{\sigma_{p.max} \cdot I_{pr} \cdot 2}{OD}$$

$$M_{p.all} = 104.689\,kNm$$

This gives that the maximum allowable tip load is:

$$Tip_{max} := \frac{M_{p.all}}{L_{prong}}$$

$$Tip_{max} = 116.321\,kN$$

Cursor beam and connection beam calculations:

The cursor beam is assumed to be fully fixed at both supports.

Cross section properties from steel table:

Cross section area: $A_{cb} := 7.45 \cdot 10^{3} mm^{2}$

Second moment of inertia: $I_{cb} := 44.2 \cdot 10^{6} mm^{4}$

Elastic section modulus: $W_{e.cb} := 442 \cdot 10^{3} mm^{3}$

Plastic section modulus: $W_{pl.cb} := 526 \cdot 10^{3} mm^{3}$

Second moment of torsion: $I_{t.cb} := 70.6 \cdot 10^{6} mm^{4}$

Calculation of cross section class of beam:

Section class:

$$Class_{c.b} := \begin{cases} "1" & \text{if } 0 \le \frac{c_{cb}}{t_{w.cb}} \le 72 \cdot \varepsilon \\ "2" & \text{if } 72 \cdot \varepsilon \le \frac{c_{cb}}{t_{w.cb}} \le 83 \varepsilon \\ "3" & \text{if } 83 \cdot \varepsilon \le \frac{c_{cb}}{t_{w.cb}} \le 124 \cdot \varepsilon \\ "4" & \text{otherwise} \end{cases}$$

$Class_{c.b} = "1"$

Moment capacity for cursor beam:

Plastic capacity:

$$M_{pl.Rd.cb} := \frac{W_{pl.cb} \cdot f_y}{\gamma_{M1}}$$

$$M_{pl.Rd.cb} = 169.755\,kNm$$

Elastic capacity:

$$M_{el.Rd.cb} := \frac{W_{e.cb} \cdot f_y}{\gamma_{M1}}$$

$$M_{el.Rd.cb} = 142.645\,kNm$$

Compression force capacity:

$$N_{cap.cb} := \frac{A_{cb} \cdot f_y}{\gamma_{M1}}$$

$$N_{cap.cb} = 2.404 \times 10^3 \cdot kN$$

Shear force capacity:

Shear area:

$$A_{v.cb} := \frac{A_{cb} \cdot h_{cb}}{h_{cb} + w_{cb}}$$

$$A_{v.cb} = 3.725 \times 10^3 \cdot mm^2$$

Plastic capacity:

$$V_{pl.Rd.cb} := \frac{A_{v.cb} \cdot f_y}{\gamma_{M1} \cdot \sqrt{3}}$$

$$V_{pl.Rd.cb} = 694.067\,kN$$

This will give the following shear force in the beam:

$$V_{cb} := \frac{6 \cdot M_{p.all} \cdot \left(\frac{L_{cb}}{2}\right)^2}{L_{cb}^3}$$

$$V_{cb} = 56.691\,kN$$

Elastic capacity check, von Mises:

First moment of area:

$$S_x := \left(\frac{h_{cb}}{2} - \frac{t_{w.cb}}{2}\right)\cdot w_{cb}\cdot t_{w.cb} + 2\cdot\left[\left(\frac{\frac{h_{cb}}{2} - t_{w.cb}}{2}\right)\cdot\left(\frac{h_{cb}}{2} - t_{w.cb}\right)\cdot t_{w.cb}\right]$$

$$S_x = 2.71\times 10^5\cdot mm^3$$

Shear stress:

$$\tau_{Ed.cb} := \frac{V_{cb}\cdot S_x}{I_{cb}\cdot t_{w.cb}}$$

$$\tau_{Ed.cb} = 34.758\,MPa$$

Maximum moment i cursor beam:

$$M_{cb} := \frac{M_{p.all}}{2}$$

$$M_{cb} = 52.344\,kNm$$

Bending stress:

$$\sigma_{cb} := \frac{M_{cb}}{I_{cb}}\cdot\frac{h_{cb}}{2}$$

$$\sigma_{cb} = 118.426\,MPa$$

von Mises criteria:

$$\sigma_{j.cb} := \sqrt{\sigma_{cb}^{\,2} + 3\cdot\tau_{Ed.cb}^{\,2}}$$

$$\sigma_{j.cb} = 132.85\,MPa$$

Elastic criteria:

$$\sigma_{d.cb} := \frac{f_y}{\gamma_{M1}}$$

$$\sigma_{d.cb} = 322.727\,MPa$$

''von Mises criteria, OK''

Since we have several combinations of loads acting on the cursor beam, we can get a reduced capacity for both moment and shear.

Moment capacity can get reduced due to shear force and compression.
Shear force can get reduced due to torsion (this is especially important for the connection beam)

Reduced moment capacity:

The moment capacity can get reduced due to shear force, if the shear force is larger than half the plastic shear resistance.
Since we do not know the actual shear force we will use a shear force from the maximum prong force.

Reduction due to shear:

$V_{Ed.cb} := V_{cb}$ $V_{Ed.cb} = 56.691\,kN$

$\frac{V_{Ed.cb}}{V_{pl.Rd.cb}} = 0.082$ ''NO reduction due to shear''

Reduction due to axial compression:

As for with shear force we also here need to assume force acting on the prong.
For this we will use the maximum tip load from the prong capacity check.

$N_{act.cb} := Tip_{mom.el.f}$

$n := \frac{N_{act.cb}}{N_{cap.cb}}$ $n = 0.049$

$a_w := \frac{\left(A_{cb} - 2 \cdot w_{cb} \cdot t_{w.cb}\right)}{A_{cb}}$ $a_w = 0.463$

Moment reduction factor: $m_{rf} := \frac{1 - n}{1 - 0.5 \cdot a_w}$

$m_{rf} = 1.238$

''NO reduction due to axial compression''

Reduced shear capacity due to torsion:

Force creating torsion:

$F_t := Tip_{max}$

$F_t = 116.321\,kN$

Torsion moment:

$T_m := F_t \cdot L_{prong}$

$T_m = 104.689\,kNm$

Torsion centre line area:

$A_m := (h_{cb} - t_{w.cb}) \cdot (w_{cb} - t_{w.cb})$

$A_m = 3.61 \times 10^4 \cdot mm^2$

Torsion shear flow:

$$\tau_{t.Ed} := \frac{T_m}{2.A_m \cdot t_{w.cb}}$$

$\tau_{t.Ed} = 144.998\,MPa$

Plastic torsion capacity:

$$V_{pl.T.Rd.cb} := \left[1 - \frac{\tau_{t.Ed}}{\frac{\left(\frac{f_y}{\sqrt{3}}\right)}{\gamma_{M1}}}\right] \cdot V_{pl.Rd.cb}$$

$V_{pl.T.Rd.cb} = 153.949\,kN$

Torsion shear flow utilization:

$$US_{T.cb} := \frac{F_t}{V_{pl.T.Rd.cb}}$$

$US_{T.cb} = 0.756$

Because of this the yield strength in the connection beam will get reduced, ref: NS3472 12.2.7

Reduced yield strength:

$$f_{y.V} = f_y \cdot (1 - \rho)$$

where:

$$\rho := \left(2 \cdot \frac{Tip_{max}}{V_{pl.T.Rd.cb}} - 1 \right)^2$$

$$\rho = 0.261$$

Yield strength in connection beam:

$$f_{y.V} := f_y \cdot (1 - \rho)$$

$$f_{y.V} = 262.246\,MPa$$

Maximum allowable bending moment in connection beam:

$$M_{max.co.b} := \frac{W_{e.cb} \cdot f_{y.V}}{\gamma_{M1}}$$

$$M_{max.co.b} = 105.375\,kNm$$

Bending moment subjected to the connection beam:

$$M_{co.b} := Tip_{max} \cdot L_{co.b}$$

$$M_{co.b} = 23.264\,kNm$$

Elastic capacity check, von Mises:

Shear stress:

$$\tau_{Ed.co.b} := \frac{Tip_{max} \cdot S_x}{I_{cb} \cdot t_{w.cb}}$$

$$\tau_{Ed.co.b} = 71.319\,MPa$$

Bending stress:

$$\sigma_{co.b} := \frac{M_{co.b}}{I_{cb}} \cdot \frac{h_{cb}}{2}$$

$$\sigma_{co.b} = 52.634\,MPa$$

von Mises criteria: $\sigma_{j.co.b} := \sqrt{\sigma_{co.b}^{2} + 3 \cdot \tau_{Ed.co.b}^{2}}$

$\sigma_{j.co.b} = 134.274\,MPa$

Elastic criteria: $\sigma_{d.co.b} := \frac{f_{y.V}}{\gamma_{M1}}$

$\sigma_{d.co.b} = 238.405\,MPa$

''von Mises criteria OK''

Maximum tip load calculated from prong, cursor beam and connection beam capacity:

$$V_{max} = \frac{6 \cdot Tip_{max.el.p} \cdot L_{prong} \cdot \left(\frac{L_{cb}}{2}\right)^{2}}{L_{cb}^{3}}$$

V.max gives that the maximum tip load that yields maximum shear is:

$$V_{pl.max.cb} := \frac{2}{3} \cdot \frac{V_{pl.Rd.cb} \cdot L_{cb}}{L_{prong}}$$

Maximum tip load for plastic and elastic capacity for prong, cursor beam and connection beam.

$$P_{max} := \min\left(\frac{M_{pl.Rd.p}}{L_{prong}}, V_{pl.cap.p}, \frac{M_{pl.Rd.cb} \cdot 2}{L_{prong}}, N_{cap.cb}, V_{pl.max.cb}, \frac{M_{p.all}}{L_{prong}}, \frac{M_{el.Rd.cb} \cdot 2}{L_{prong}}\right)$$

$P_{max} = 116.321\,kN$

P.max in tonnes: $P_{max.Te} := \frac{P_{max}}{g}$

$P_{max.Te} = 11.861\,Te$

This gives that the prong is the weakest member with a capacity of 11.86Te tip load. This is without load factor and only to be used in further Staad.Pro analysis.

Bolt and weld capacity check:

Bolt:

The prongs are connected to the cursor beam by bolted plates and the cursor beam is connected to the cursor frame with bolted plates. There are four bolts which will get affected by the tip loads on the prong. These bolts will experience; tension and compression (from the moment), shear forces and torsion.

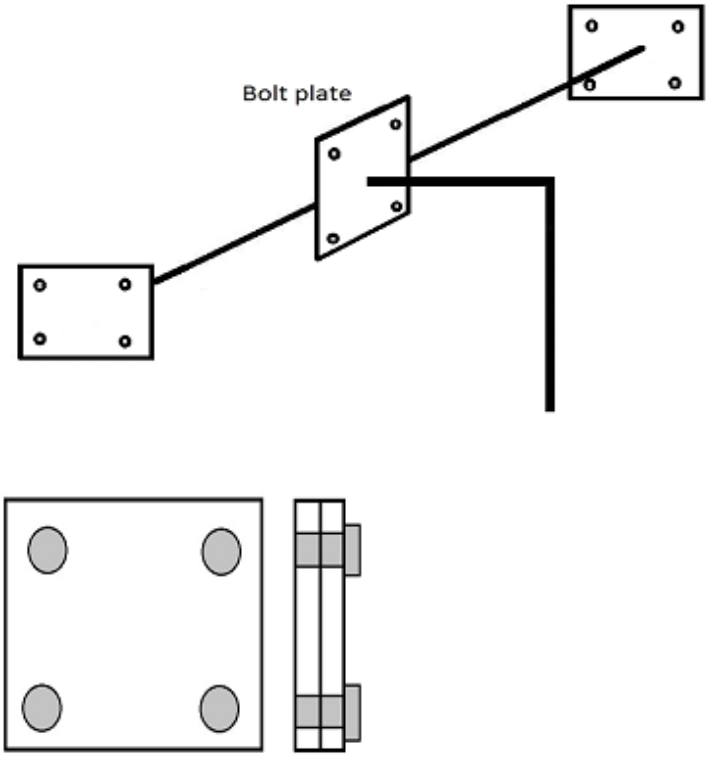

The bolts are M24 x 80, Steel grade: 8.8

$f_{u.b} := 800\text{MPa}$

Yield strength bolts:

$$f_{y.b} := \frac{8}{10} \cdot f_{u.b}$$

$$f_{y.b} = 640 \cdot \text{MPa}$$

Plate properties:

$f_{y.p} := f_y$

$f_{y.p} = 355 \cdot MPa$

$f_{u.p} := 490MPa$

Material factors:

$\gamma_{M2} := \gamma_{M2}$

$\gamma_{M2} = 1.25$

We check the bolts for rip out and cut off, and we will check for rapture of the plate which the bolts are connected to.

Capacity of the plate material alone:

Plate thickness:

$t_p := 15mm$

Plate width:

$w_p := 390mm$

Area of plate affected by shear:

$A_p := t_p \cdot w_p$

$A_p = 5.85 \times 10^3 \cdot mm^2$

Plate capacity for shear force:

$$N_{cap.plate} := \frac{f_{y.p}}{\gamma_{M1}} \cdot A_p$$

$N_{cap.plate} = 1.888 \times 10^3 \cdot kN$

Reduction due to bolt holes:

If we consider the shear force as a axial force acting on the plate, there will be 2 bolts that can reduce the capacity (due to the holes).

Bolt diameter:

$d_0 := 26mm$

Reduced area:

$A_{red} := A_p - 2 \cdot d_0 \cdot t_p$

$A_{red} = 5.07 \times 10^3 \cdot mm^2$

Reduced plate capacity:

$$N_{red.cap.plate} := 0.9 \cdot \left(\frac{f_{u.p}}{\gamma_{M2}} \cdot A_{red} \right)$$

$N_{red.cap.plate} = 1.789 \times 10^3 \cdot kN$

Bolt cut off due to shear force:

Number of bolts affected by the tip load: $n_1 := 4$

Bolt area: $A_{bolt} := \frac{\pi \cdot d_0^2}{4}$

$A_{bolt} = 530.929\,mm^2$

Total bolt capacity: $F_{cap.bolt} := n_1 \cdot \frac{0.6 \cdot f_{u.b} \cdot A_{bolt}}{\gamma_{M2}}$

$F_{cap.bolt} = 815.507\,kN$

Capacity with respect to the pressure at the bolt hole edge:

We assume that the bolt hole is the bolt diameter plus 2 mm.

Bolt hole: $d_{bh} := d_0 + 2mm$

$d_{bh} = 28 \cdot mm$

Distances in the load direction:

$e_1 := 30mm$ $\quad if(e_1 > 1.2 \cdot d_{bh}, "e.1 \text{ is OK}", "e.1 \text{ is NOT OK}") = "e.1 \text{ is NOT OK}"$

$p_1 := 260mm$ $\quad if(p_1 > 2.2 \cdot d_{bh}, "p.1 \text{ is OK}", "p.1 \text{ is NOT OK}") = "p.1 \text{ is OK}"$

$e_2 := 30mm$ $\quad if(e_2 > 1.2 \cdot d_{bh}, "e.2 \text{ is OK}", "e.2 \text{ is NOT OK}") = "e.2 \text{ is NOT OK}"$

$p_2 := 330mm$ $\quad if(p_2 > 2.4 \cdot d_{bh}, "p.2 \text{ is OK}", "p.2 \text{ is NOT OK}") = "p.2 \text{ is OK}"$

This shows us that the edge distances e.1 and e.2 are too small. But since these dimensions are used today, these dimensions are used in further calculations.

$$\alpha_{min} := \min\left(\frac{e_1}{3 \cdot d_{bh}}, \frac{p_1}{3 \cdot d_{bh}} - \frac{1}{4}, \frac{f_{u.b}}{f_{u.p}}, 1\right)$$

$\alpha_{min} = 0.357$

Bolt reduction factor:

$$c_1 := \frac{e_2}{0.9 \cdot d_{bh}} - \frac{2}{3}$$

$$c_1 = 0.524$$

Bolt capacity with respect to bolt edge pressure:

$$F_{bo.ed} := \frac{2.5 \cdot \alpha_{min} \cdot f_{u.b} \cdot d_0 \cdot t_p}{\gamma_{M2}} \cdot c_1 \cdot n_1$$

$$F_{bo.ed} = 466.939\,kN$$

All capacity for bolts and the plate calculated above is with respect to the shear force generated by the tip force on the prong.

Max load for bolt and plate capacity:

$$Min_{bolt.cap} := \min\left(N_{red.cap.plate}, F_{cap.bolt}, F_{bo.ed}\right) = 466.939\,kN$$

The bolt hole edge pressure yields bolt capacity.

This gives a maximum tip load with regards to bolt capacity of:

$$F_{tip.cap.bolt} := \frac{2}{3} \cdot \frac{Min_{bolt.cap} \cdot L_{cb}}{L_{prong}}$$

$$F_{tip.cap.bolt} = 958.089\,kN$$

When the tip loads come from the direction with 90 degree angle to the cursor beam we will experience tension in the 2 upper bolts of the plate.

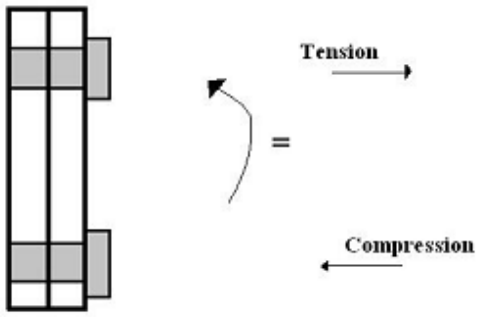

Number of bolts subjected to tension:

$$n_2 := 2$$

Bolt capacity for tension force:

$$F_{d.t} := n_2 \cdot \frac{0.9 \cdot f_{u.b} \cdot A_{bolt}}{\gamma_{M2}} = 611.63\,kN$$

Weld:

For the weld, maximum prong load is applied.

The shear force acting on the weld: $V_{weld} := P_{max}$

$V_{weld} = 116.321\,kN$

The moment acting on the weld: $M_{weld} := M_{p.all}$

$M_{weld} = 104.689\,kNm$

Root size of the weld: $a_{weld} := 7mm$

Correlation factor for the weld (S355): $\beta_w := 0.9$

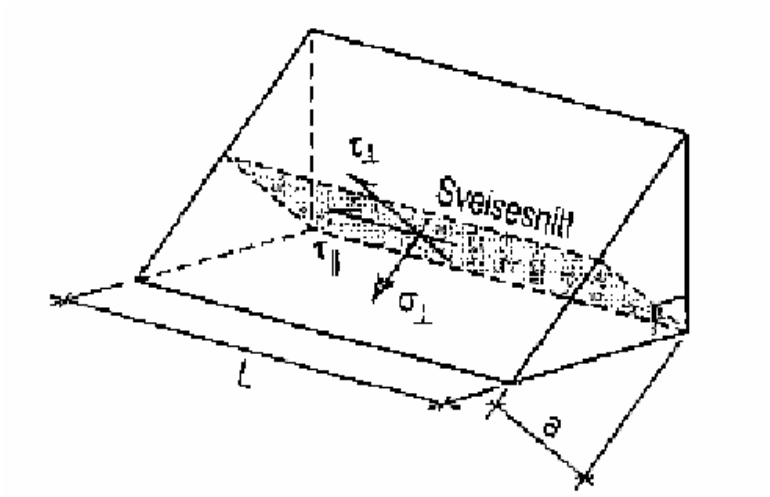

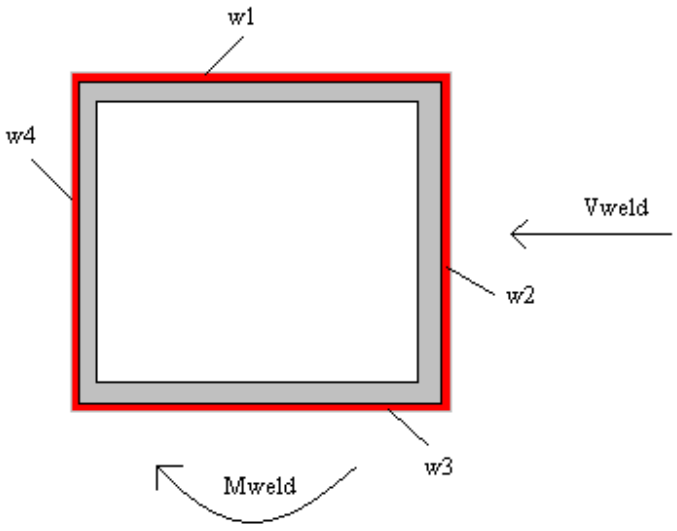

Since the welds on different sides of the beam will get affected in different ways, they have been separated into 4 single welds.

Lengths of weld: $L_{w1} := 200mm$ $L_{w2} := 200mm$

$L_{w3} := 200mm$ $L_{w4} := 200mm$

Areas of welds: $A_{w1} := L_{w1} \cdot a_{weld} = 1400 \cdot mm^2$

$A_{w2} := L_{w2} \cdot a_{weld} = 1400 \cdot mm^2$

$A_{w3} := L_{w3} \cdot a_{weld} = 1400 \cdot mm^2$

$A_{w4} := L_{w4} \cdot a_{weld} = 1400 \cdot mm^2$

Bending tension i the weld due to moment is:

$$\sigma_{M.weld} = \frac{M_{weld}}{\sum_4 I_{weld.i}} \cdot z_{weld}$$

Largest distance from the NA axis of the beam: $z_{weld} := \frac{h_{cb}}{2} + \frac{a_{weld}}{2}$

$z_{weld} = 103.5mm$

2. moment of inertia for each weld:

$I_{weld.1} := \frac{a_{weld} \cdot L_{w1}^3}{12}$ $I_{weld.1} = 4.667 \times 10^6 \cdot mm^4$

$I_{weld.2} := \frac{L_{w2} \cdot a_{weld}^3}{12} + L_{w2} \cdot a_{weld} \cdot z_{weld}^2$ $I_{weld.2} = 1.5 \times 10^7 \cdot mm^4$

$I_{weld.3} := \frac{a_{weld} \cdot L_{w3}^3}{12}$ $I_{weld.3} = 4.667 \times 10^6 \cdot mm^4$

$I_{weld.4} := \frac{L_{w4} \cdot a_{weld}^3}{12} + L_{w4} \cdot a_{weld} \cdot z_{weld}^2$ $I_{weld.4} = 1.5 \times 10^7 \cdot mm^4$

Total 2.moment of inertia of all the welds:

$$I_{weld} := I_{weld.1} + I_{weld.2} + I_{weld.3} + I_{weld.4}$$

$$I_{weld} = 3.934 \times 10^{7} \cdot mm^{4}$$

Maximum bending stress due to moment:

$$\sigma_{M.weld} := \frac{M_{weld}}{I_{weld}} \cdot z_{weld} \qquad \sigma_{M.weld} = 275.433\,MPa$$

Decomposed we get:

$$\sigma_{M.90deg} := \frac{\sigma_{M.weld}}{\sqrt{2}} \qquad \sigma_{M.90deg} = 194.76\,MPa$$

$$\tau_{M.90deg} := \frac{\sigma_{M.weld}}{\sqrt{2}} \qquad \tau_{M.90deg} = 194.76\,MPa$$

The shear force will give shear stresses in the welds (parallel to the force direction)

$$\tau_{V.0deg} := \frac{V_{weld}}{A_{w1} + A_{w3}} \qquad \tau_{V.0deg} = 41.543\,MPa$$

von Mises criteria for welds give:

$$\sigma_{j.weld} := \sqrt{\sigma_{M.90deg}^{2} + 3 \cdot \left(\tau_{M.90deg}^{2} + \tau_{V.0deg}^{2}\right)}$$

$$\sigma_{j.weld} = 396.111\,MPa$$

Criteria:

$$cri_{weld} := \frac{f_{u.p}}{\gamma_{M2} \cdot \beta_{w}} = 435.556\,MPa$$

$$\sqrt{\sigma_{\perp}^2 + 3\left(\tau_{\perp}^2 + \tau_{\parallel}^2\right)} \leq \frac{f_u}{\gamma_{M2}\beta_w}$$

$$\sigma_{\perp} \leq \frac{f_u}{\gamma_{M2}}$$

Criteria check:

$\text{Criteria}_{check} := \text{if}\left(\text{cri}_{weld} \geq \sigma_{j.weld}, \text{"The weld capacity is OK"}, \text{"The weld will break before the prong"}\right)$

$\text{Criteria}_{check} = \text{"The weld capacity is OK"}$

Weld utilization: $\text{US}_{weld} := \frac{\sigma_{j.weld}}{\text{cri}_{weld}}$

$\text{US}_{weld} = 0.909$

The maximum tip load utilize 90.9% of the weld capacity.

Appendix II: Impulse load calculations – Stiff vs. flexible prong

Weight of running tool: $m_{tool} := 40000kg$

Impact speed: $v_1 := 0.05\frac{m}{s}$

End speed: $v_2 := 0\frac{m}{s}$

1. Stiff prong

To calculate the impact load we look at the change in quantity of motion. The impact at the stiff prong is assumed to stop during a time interval of 0.6 s. This correspond to a deflection of 30 mm and a deflection speed of 0.05 m/s.

Time interval: $\Delta t_1 := 0.6s$

Change in quantity of motion: $m_{tool} \cdot v_2 - m_{tool} \cdot v_1 = -2 \times 10^3 \frac{m \cdot kg}{s}$

Average load on prong: $J_1 = F_{av.2} \cdot \Delta t_1 = m_{tool} \cdot v_2 - m_{tool} \cdot v_1$

$$F_{av.1} := \frac{m_{tool} \cdot v_2 - m_{tool} \cdot v_1}{\Delta t_1}$$

$$F_{av.1} = -3.333 \times 10^3 N$$

2. Flexible prong

The impact at the flexible prong is assumed to stop during a time interval of 1.6 s. This correspond to a deflection of 80 mm and a deflection speed of 0.05 m/s.

Time interval: $\Delta t_2 := 1.6s$

Change in quantity of motion: $m_{tool} \cdot v_2 - m_{tool} \cdot v_1 = -2 \times 10^3 \frac{m \cdot kg}{s}$

Average load on prong:

$$J_1 = F_{av.2} \cdot \Delta t_2 = m_{tool} \cdot v_2 - m_{tool} \cdot v_1$$

$$F_{av.2} := \frac{m_{tool} \cdot v_2 - m_{tool} \cdot v_1}{\Delta t_2}$$

$$F_{av.2} = -1.25 \times 10^3 \text{ N}$$

Change of impulse loading:

$$\Delta := \frac{F_{av.1} - F_{av.2}}{F_{av.1}}$$

$$\Delta = 0.625$$

This shows that the flexible prong will experience a impulse loading which 62.5% lower than with the stiff prong.

All of these calculations are rough so detailed time domain dynamic calculations are recommended

Appendix III: Maximum pitch angle

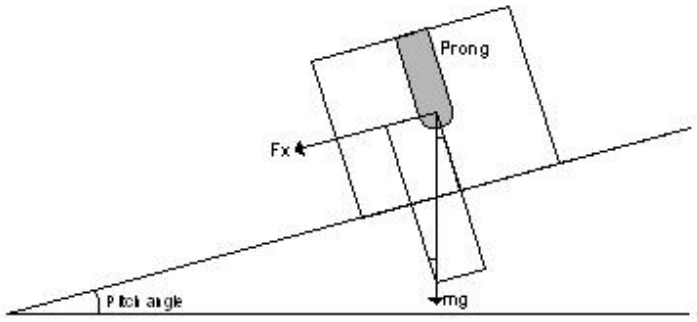

Maximum static tip load on prong: $F_{max} := 11500\,kg$

Weight of running tool: $m_{tool} := 40000\,kg$

Decompose of force: $F_x = m \cdot g \cdot \sin(\alpha)$

Maximum pitch angle: $\alpha_{max} := \operatorname{asin}\left(\frac{F_{max} \cdot g}{m_{tool} \cdot g}\right)$

$\alpha_{max} = 16.708\,deg$

This gives that each prong can take an angle of 16.7 degree in pitch.

Appendix IV: Flexible prong following vessel motion

The illustration shows how the flexible prong will behave when the vessel has a motion less than 5 degrees in any direction. Instead of risking over stressed guide wires and stuck prongs, the flexible prong will follow the vessels motion.